Meridional Heat Transport Variability at 26.5°N in the North Atlantic

EVE R. FILLENBAUM, THOMAS N. LEE, WILLIAM E. JOHNS, AND RAINER J. ZANTOPP

Rosenstiel School of Marine and Atmospheric Science, University of Miami, Miami, Florida

(Manuscript received 27 June 1995, in final form 31 July 1996)

ABSTRACT

Data from almost five years of current meter moorings located across the Bahamas Escarpment at 26.5°N are used to investigate meridional heat transport variability in the section and its impact on transatlantic heat flux. Estimates of heat transport derived from the moored arrays are compared to results from the Community Modeling Effort (CME) Atlantic basin model and to historical hydrographic section data. A large fraction of the entire transatlantic heat flux is observed in this western boundary region, due to the opposing warm and cold water flows associated with the Antilles Current in the thermocline and the deep western boundary current at depth. Local heat transport time series derived from the moored arrays exhibit large variability over a range of ± 2 PW relative to 0°C, on timescales of roughly 100 days. An annual cycle of local heat transport with a range of 1.4 PW is observed with a summer maximum and fall minimum, qualitatively similar to CME model results. Breakdown of the total heat transport into conventional ''barotropic'' (depth averaged) and ''baroclinic'' (transport independent) components indicates an approximately equal contribution from both components. The annual mean value of the baroclinic heat transport in the western boundary layer is 0.53 ± 0.08 PW northward, of opposite direction and more than half the magnitude of the total southward baroclinic heat transport between Africa and the Bahamas (about −0.8 PW) derived from transatlantic sections. Combination of the results from the moored arrays with Levitus climatology in the interior and historical Florida Current data yields an estimate of 1.44 ± 0.33 PW for the annual mean transatlantic heat flux at 26.5°N, approximately 0.2 PW greater than the previously accepted value of 1.2–1.3 PW at this latitude.

1. Introduction

Determining the patterns and amounts of heat transported in the World Ocean is of great importance to our understanding of ocean circulation and its influence on climate variability. Oceanic heat flux is closely coupled to the deep (thermohaline forced) circulation, the formation of water masses, and global climate. Heat transport by the oceans is thought to play a major role in climate moderation (Vonder Haar and Oort 1973). Because the timescales on which the oceans transport heat are so much longer than those in the atmosphere, and because the oceans serve as a giant heat sink or ''flywheel'' for the global heat cycle, the oceans play an important role in climate change. Recent coupled ocean–atmosphere models imply that there are at least two stable states for ocean circulation and atmospheric climate: one state with a fairly intense thermohaline circulation, large oceanic heat transport, and a fairly moderate climate similar to that currently existing, and another state with weaker circulation, less heat transport, and an ice-age climate (Bryan 1986; Manabe and Stouffer 1988).

Oceanic heat flux has typically been calculated from rather sparse data, widely and unevenly distributed in time and space. Typically, estimates of net ocean heat flux have been made using single hydrographic sections, which are assumed to be representative of the mean state of the ocean. Here long-term time series of velocity and temperature from current meter moorings deployed east of Abaco Island at 26.5°N (Fig. 1) are used to investigate the influence of western boundary current variability on transatlantic heat flux on timescales from monthly to interannual.

A recent paper by Lee et al. (1996, hereafter LJZF) describes the structure and variability of these currents and their relationship to basinwide wind and thermohaline forcing. A similar quantitative understanding of heat transport variability in this western boundary current region will enable us to improve traditional heat flux measurements made from hydrographic sections or ship of opportunity data. As noted by Hall and Bryden (1982), errors in estimating the transport of western boundary currents on continental slopes and over shallow regions can introduce large errors in meridional oceanic heat flux estimates. The Abaco dataset provides an opportunity to directly compute the heat transport on

Corresponding author address: Dr. Eve R. Fillenbaum, NRL Code 7332, Stennis Space Center, MS 39529.
E-mail: fillenbaum@nrlssc.navy.mil

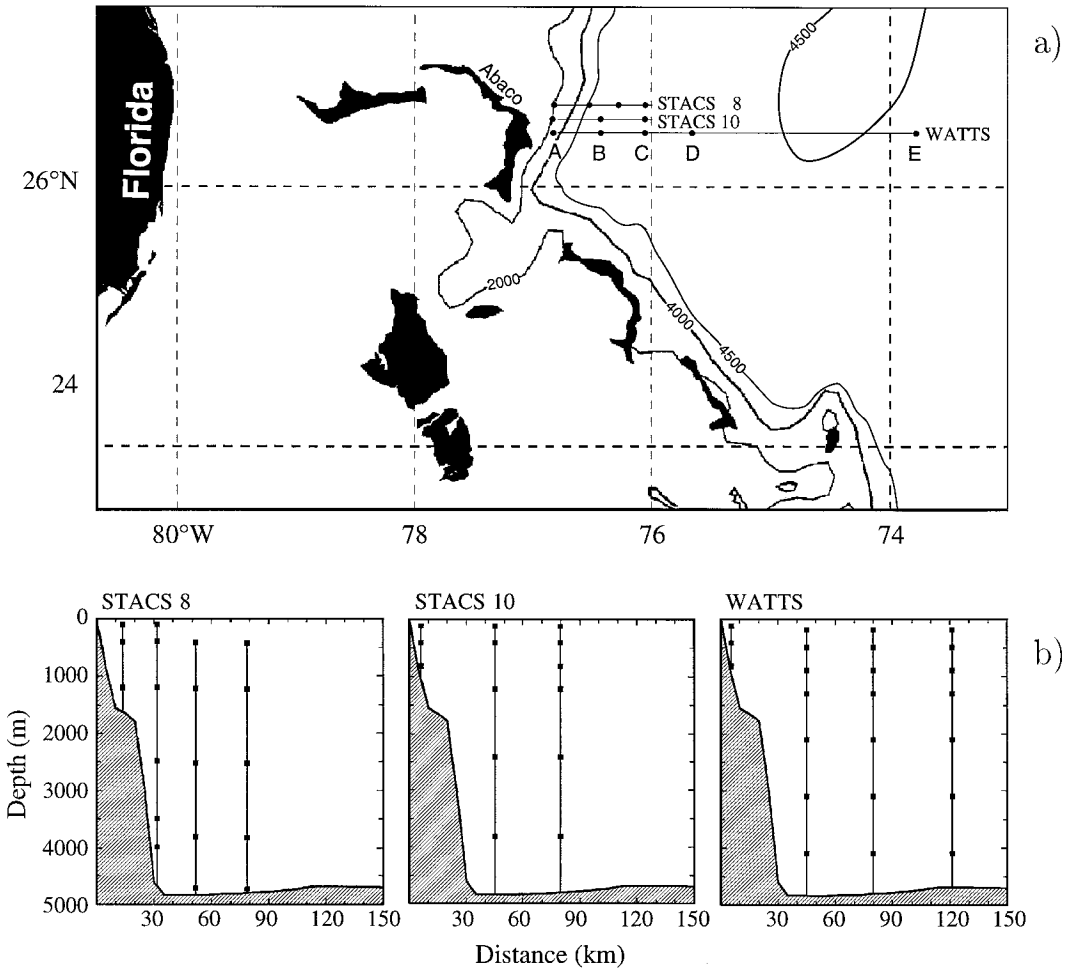

FIG. 1. (a) Array locations for STACS-8, STACS-10, and WATTS. The WATTS array extends farther east than the earlier deployments. Locations are shown spread in latitude for clarity; all moorings are actually located very close to 26.5°N. (b) Mooring locations and instrument depths for each deployment are shown below.

the continental slope, as well as a means of estimating the eddy heat flux in this area.

The organization of this paper will be as follows: After this introduction to heat transport and regional circulation, section 2 (methods) deals with a description of mooring and model data, correction of mooring data, and methods of calculating the heat transport. In section 3 (results) we present time series of heat transport, discuss their variability, and investigate the annual cycle in observed heat transport. We also consider onshore and offshore positions of the deep western boundary current, as these can affect the volume and heat transports derived from the moored data. In section 4 (discussion), we consider implications for transatlantic section heat flux and discuss differences between modeled and observed results. Section 5 presents a summary of results and conclusions.

Meridional heat flux in the Atlantic is dominated by the large-scale overturning cell that transports deep water southward across the equator into the Southern Ocean, balanced by a warm return flow in the thermocline. The dominance of meridional overturning is primarily because temperature differences in the ocean are typically much greater within the water column than horizontally. Thus, it is the thermohaline circulation, with its associated overturning and deep circulation, that plays a major role in transporting heat. Roemmich and Wunsch (1985), for example, found that the wind-driven circulation accounts for less than 10% of the heat flux through 24°N in the North Atlantic. Because the thermohaline circulation is weaker in the Pacific than in the Atlantic (partly because little or no deep water is formed in the Pacific), the meridional heat flux is weaker; it has been measured at 0.76 PW across 24°N in the Pacific, which is less than two-thirds the corresponding value in the Atlantic (Bryden et al. 1991).

For practical purposes, meridional heat flux is defined by the integral

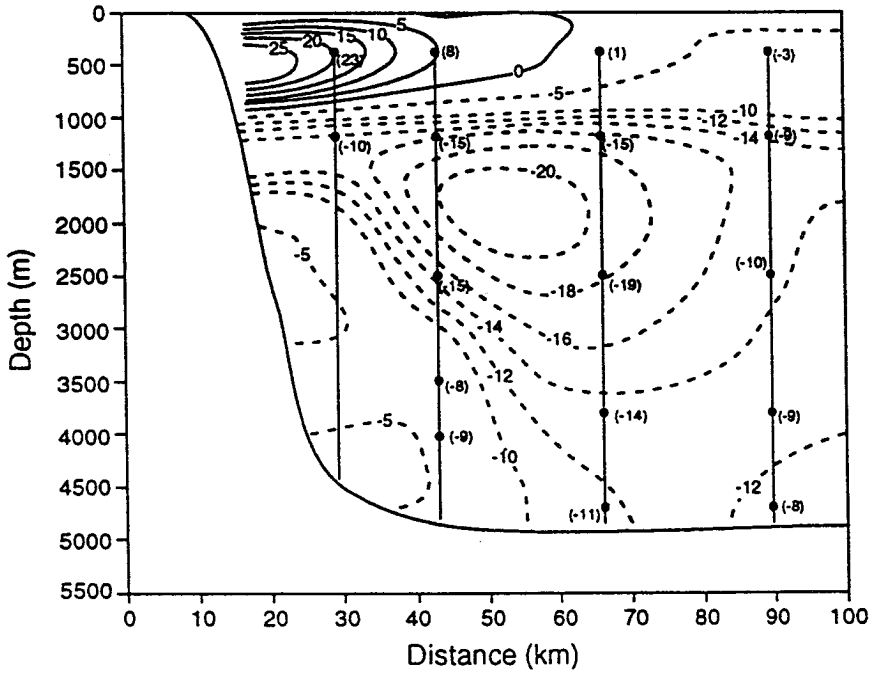

FIG. 2. Average geostrophic velocity referenced by Pegasus absolute velocities for April 1985–September 1987 over the mooring area (after Lee et al. 1990).

$$\int_0^H \int_0^L C_p \rho v \theta \, dx \, dz, \tag{1}$$

(Bryan 1962) where C_p is the heat capacity of the ocean at constant pressure, ρ is the water density, θ is the potential temperature (measured in °C), v is the north–south component of velocity, L is the width of the ocean at the latitude being considered, and H is the ocean depth, which can vary across the section. The product $C_p\rho$ is normally assumed constant. Oceanic heat flux is normally expressed in petawatts (PW), where 1 PW = 10^{15}W. A meaningful estimate of the meridional ocean heat flux requires the calculation of (1) over a full oceanic section for which there is zero net mass transport; otherwise the calculated heat transport is dependent on an arbitrary temperature reference. This is nearly true for the Atlantic, which is closed to the north except for a small transport occurring through the Bering Strait that negligibly affects the heat flux calculation at midlatitudes (Hall and Bryden 1982).

We will use moored transport estimates, along with results from the Community Modeling Effort model (CME) to describe the influence of western boundary currents off Abaco, Bahamas, on the transatlantic heat flux. The boundary currents off Abaco are characterized by two major flow regimes, divided vertically near 800 m where the mean meridional flow reverses from northward in the upper ocean to southward at depth (Fig. 2). In the upper layer, a mean Antilles Current is observed with a warm northward core at an average depth of 400 m, located close to the Bahamas Escarpment (Lee et al. 1990). In LJZF it is concluded that the Antilles Current is necessary as part of the western boundary current closure of the wind-driven subtropical gyre, but does not appear to be involved in interhemispheric exchange—that is, it is not part of the thermohaline circulation (see also Schmitz et al. 1992). Flow below 800 m is dominated by a strong deep western boundary current (DWBC) with a southward core centered near 2500 m approximately 25 km seaward of the boundary. LJZF reported considerable variability in the strength and position of these currents, causing large decreases in the observed total southward transport at times when the DWBC meanders offshore and becomes only partially resolved by the moored arrays. LJZF also found a large annual cycle of meridional transports off the Bahamas [$\pm$ 13 Sv (Sv $\equiv 10^6$ m^3 s^{-1}), with maximum northward transports in winter and summer and minima in fall and spring] that agrees in magnitude and phase with that predicted by wind-forced basin models. The mean southward transport of the DWBC reported by LJZF, of approximately 40 Sv, is two to three times larger than the accepted values for net interhemispheric exchange, indicating a large recirculating component. Volume transports through the section ranged from 80 Sv southward to 60 Sv northward, and the DWBC core was seen to meander from 25 to 125 km offshore. The dominant timescale of variability was 70 to 100 days, with the major causes of variability believed to be meandering of the DWBC and propagation of baroclinic upper-ocean eddies into the region from the interior. The reader is referred to LJZF for more complete discussion of the

structure and variability of the Abaco western boundary current regime.

2. Methods

a. Moored current meter measurement

The results are primarily based on data from three moored current meter arrays that were deployed at 26.5°N off Abaco Island from April 1987 to February 1992 (Fig. 1). These arrays are referred to from earliest to latest as STACS-8 (consisting of four moorings deployed from Apr 1987 to Jun 1988), STACS-10 (three moorings, Oct 1988–Jun 1990), and WATTS (five moorings, Jun 1990–Feb 1992). The first two settings were part of the NOAA/AOML SubTropical Atlantic Climate Studies project, while the third was from the NSF sponsored Western Atlantic Thermohaline Transport Study. There were typically six or seven instruments per mooring, all measuring velocity and temperature, and usually two per mooring with pressure sensors. Instruments were located nominally at 100, 400, 1200, 2500, 3800, and 4700 m for STACS-8 and STACS-10, and 100, 400, 800, 1200, 2000, 3000, and 4000 m for WATTS (Fig. 1b). The westernmost mooring in each array was in shallower water on the upper Bahamian slope (900 to 1600 m), with deepest instruments at 800 or 1200 m. The coherent part of the array, extending from the Bahamas boundary to approximately 85 km offshore, was designed to observe volume and heat transports of the concentrated western boundary flows.

Measured current, temperature, and pressure time series from the moored instruments were edited to fill gaps and remove spikes, then filtered with a 40-h low-pass filter to remove the effect of tides. Resulting time series of u (positive east) and v (positive north) components of velocity, in situ temperature, and pressure were then subsampled every 12 h.

b. Correction for mooring motion

Locally strong barotropic currents off Abaco caused considerable mooring setdown with vertical displacements reaching 240 m. The measured pressure records were used to correct current and temperature time series for this mooring motion. Velocity correction was a straightforward interpolation every 25 m at each 12-h time interval using an Akima (1970) shape-preserving cubic spline fit between the known instrument depth levels. Above the shallowest instrument, the shear at the top instrument derived from the spline fit was used to extrapolate values to the surface; the bottom velocity was assumed to be zero. Moored transports calculated using this methodology have been shown to be accurate to within a few Sverdrups compared to independent estimates derived from Pegasus velocity profile sections (Lee et al. 1990; Leaman and Harris 1990).

To accomplish the temperature correction, a seasonally varying vertical temperature gradient field $dT/dp(T)$ was constructed, using data from CTD casts taken in the vicinity during the mooring deployment cruises. Using this gradient field, a corrected temperature time series was constructed for each instrument, starting with the known temperature and pressure at each time for each instrument and numerically integrating up or down to the nominal instrument depth. That is, the corrected temperature T_c at the desired pressure level p_c is given by

$$T_c = T_0 + \int_{p_0}^{p_c} \frac{dT}{dp}\, dp, \tag{2}$$

where T_0 and p_0 are the original temperature and pressure and dT/dp is a function of temperature, which is allowed to vary every tenth of a degree. To create temperature time series at arbitrary vertical resolution throughout the water column for each mooring, a similar approach was used, with a distance-weighted average of the temperature calculated from the two nearest instruments being used for any given level (for example, a 200-m time series would be constructed from the 100- and 400-m instruments). This procedure yields a smooth temperature profile that passes through the measured temperature points and is otherwise consistent with the monthly mean vertical stratification for the region. These moored temperature profiles were then compared to CTD temperature profiles taken nearby at the same time, where available; the agreement was good (see Fig. 3a for a comparison of one such constructed profile to a CTD temperature profile).

Maximum discrepancies were approximately 1.5°C (and only in the shallowest part of the profile), with typical maximum discrepancies closer to 0.5°C. Figure 3b shows the mean difference (for 24 comparisons) between CTD casts and the moored temperature profiles, with one standard deviation above and below the average difference also shown. The upper hundred meters have a low bias for the moorings (as the surface temperature is never allowed to exceed the monthly mean sea surface temperature), while the thermocline is biased slightly high by $O(0.2°C)$. These uncertainties lead to small errors in heat transport. For example, a bias error of 0.5° in temperature over the full water column, associated with a volume transport of 30 Sv, leads to a heat transport error of only 0.06 PW.

c. CME model

Results were obtained from the last 5 years of a 25-yr run of the Community Modeling Effort (CME) model performed at NCAR. This model (Bryan and Holland 1989) covers the North Atlantic from 15°S to 65°N and was adapted from the Bryan (1969) and Cox (1985) model. The CME model is semi-eddy-resolving, with a grid spacing of ⅓° in latitude by ⅖° in longitude, 30 levels in the vertical, and layer thicknesses increasing from 35 m at the surface to 250 m at the bottom. The model time step was 12 h, with results sampled every

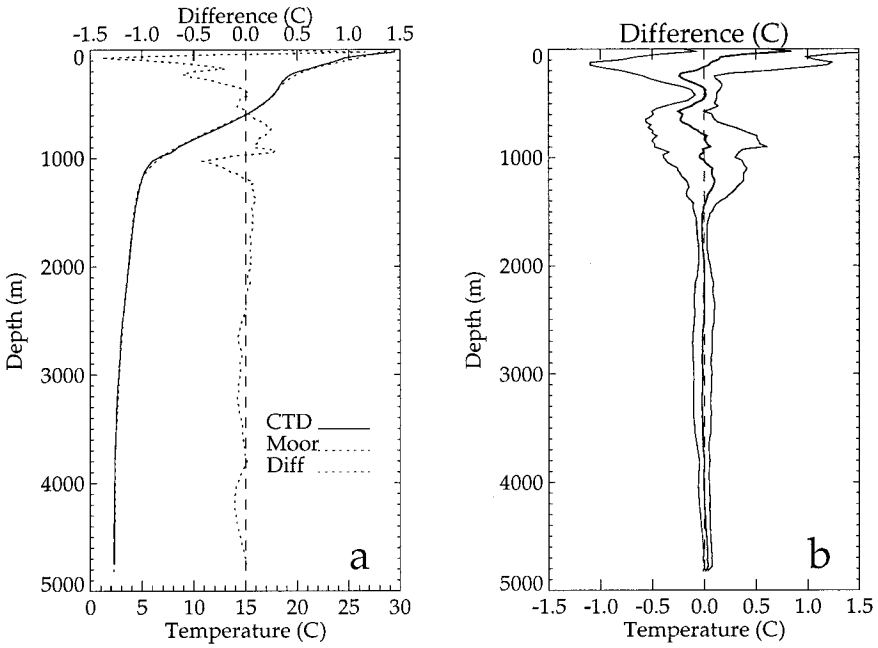

FIG. 3. (a) Comparison of CTD temperature profile (solid) to mooring temperature profile (dotted). The difference (CTD − mooring) is also shown. (b) Mean difference between CTD temperature profiles and mooring temperature profiles (bold); one standard deviation above and below the mean are indicated in light lines.

72.96 hours. These ''3-day'' values of model-derived potential temperature and meridional velocity are used to compute heat transports and can cause model time series to appear somewhat smoother than those derived from the moorings. This version of the model was forced with seasonally varying Hellerman and Rosenstein (1983) winds and Han (1984) surface fluxes. Boundary and initial conditions are based on Levitus (1982) climatology, with sponge layers at the northern and southern boundaries.

The thermohaline circulation in this version of the model has been shown to be too weak causing its meridional heat transports to be too small [0.6 PW at 26.5°N, as opposed to an accepted value of about 1.2 PW; Bryan and Holland (1989)]. Also, the wind-forced circulation appears to be stronger in the Bahamas region than that observed by the mooring arrays, as will be further discussed.

However, the model's extensive areal coverage and similar variability scales make it a useful comparison tool. Work is currently underway on improving the model circulation by changing model parameters and forcing (Böning et al. 1991a,b, 1994). The five years of model data used here are arbitrary and are not forced by actual wind stress from the years 1987 to 1992; therefore, it is the timescale and amplitude of variability and the statistical properties of the flow and temperature fields, rather than the actual events, that can be compared to the mooring results.

d. Methods of calculating heat transport

There are several possible methods for calculating heat transport. Historically, it has been calculated from ocean surface heat budgets, or as the residual of the radiation balance at the top of the atmosphere and the atmospheric heat transport. Here we will consider only what has traditionally been referred to as the ''direct'' method.

In the direct method, measured values of water velocity and potential temperature across the full width and depth of a transatlantic section are integrated according to Eq. (1) to determine the meridional heat flux. Normally, hydrographic section results are used, so the velocities are geostrophic rather than absolute. This raises the problem of referencing the geostrophic currents since the barotropic component is unresolved.

Bryden and Hall (1980) and Hall and Bryden (1982) introduced the concept of ''baroclinic'' and ''barotropic'' contributions to the total heat flux Q:

$$Q = \rho C_p \left\{ \int_0^L H\bar{v}\bar{\theta}\, dx + \int_0^L \int_0^{H(x)} v'\theta'\, dz\, dx \right\}. \quad (3)$$

Here an overbar denotes a depth average and a prime denotes a deviation from that average, H is the ocean depth, and the other terms are as previously defined. The first integral is the barotropic or depth-averaged component of heat flux, and the second is the depth-dependent baroclinic component. Thus, ''barotropic''

heat transports are those calculated by using an instantaneous depth average over the full water column for the velocity and temperature, while ''baroclinic'' heat transports use the deviations from the depth average at each point over the water column. Baroclinic volume transports are zero by definition, and baroclinic heat transports can be considered independent of any reference velocity.

Bryden and Hall (1980) also developed the breakdown into components that has become the canonical direct method. To resolve the referencing difficulty, they assume that measured northward flow through the Straits of Florida is balanced by an equivalent southward flow through the ocean interior at an interior mean temperature (i.e., that there is a mass balance of the barotropic flows). They then use baroclinic potential temperatures and geostrophic velocities in the ocean interior and assume that the upper layer Ekman flow (at a mean upper layer temperature) is balanced by a deeper return flow at the mean interior temperature. Using direct current observations from the Straits of Florida plus 1957 IGY section data (from an October hydrographic section at 24.5°N), they find a net northward heat flux of 1.22 ± 0.3 PW at 25°N in the Atlantic (Hall and Bryden 1982).

Roemmich and Wunsch (1985), using hydrographic results from their 1981 *Atlantis II* section at 24.5°N and compensating mass balances, find a heat flux of 1.2 PW. They also obtained the same result using the 1957 IGY section.

Molinari et al. (1990) (hereafter M90) studied the heat flux at 26.5°N and were the first to consider seasonal variability. Using Levitus climatology data in the interior of the ocean combined with direct velocity and temperature observations in the Straits of Florida, they find a mean value of 1.21 ± 0.34 PW for the heat flux, ranging from a low of 0.69 PW in February to a high of 1.86 PW in July.

e. Moored estimates of heat transport

The moored current meter data considered here are ideally suited to the direct method of calculating heat transport, especially as they eliminate the problem of referencing geostrophic velocities. However, since these measurements cover only a part of the transatlantic section, which in general will have a nonzero net meridional transport, heat transport estimates must be calculated relative to an arbitrary temperature reference. All calculations reported here for the Abaco moored array are referenced to 0°C, which is the standard reference used in earlier works (Hall and Bryden 1982; M90) and which allows the measurements from the Abaco array to be readily combined with available estimates for other parts of the section (e.g., the Florida Current) using the same temperature reference.

Therefore, we refer to the quantity

$$\int_0^H \int_{x_1}^{x_2} C_p \rho v \theta \, dx \, dz \tag{4}$$

computed over only part of the transatlantic section (from longitude x_1 to x_2), with θ in degrees Celcius, as a *temperature transport,* while we reserve the term *heat flux* for the equivalent quantity computed over the entire section. The former quantity has been referred to as the *temperature flux* by Hall and Bryden (1982), and the latter is frequently referred to as the *heat transport* as well as the *heat flux.*

The temperature transport through the moored array was found by creating cross sections of corrected potential temperature θ and mooring-motion-corrected velocity at 12-h intervals over the whole mooring array, using a standardized coherent section length of 85 km. These fields were interpolated to every 100 m vertically and every 5 km horizontally; potential temperatures (in °C) were calculated from the corrected in situ temperatures by using the CTD background salinity. The product $v\theta$ was then summed over the array and multiplied by $C_p\rho$ (for which we use the value 4.09773×10^6 J K^{-1} m^{-3}) to create temperature transport time series. These transport time series were then decomposed into components. That is, the temperature transports above and below 800 m were computed, as were the barotropic and baroclinic components.

Mooring coverage of the coherent portion of the array varied; four moorings were located within the coherent section during STACS-8, while only three were deployed during STACS-10 and WATTS. As discussed by LJZF, it was found that this varying coverage caused the interpolated transports to be slightly weaker when only three moorings were present, due to marginal resolution of the DWBC core. To account for this, LJZF computed a linear regression between the actual STACS-8 transport values and those from a subsampled three-mooring configuration equivalent to that used later during STACS-10 and WATTS and applied this linear correlation to the volume transport time series for the later deployments. The correlation coefficient was high (0.98), and the three-mooring configuration underestimated the southward transport by a mean value of 3 Sv. The same approach was used here to adjust the temperature transport values during STACS-10 and WATTS. As with the volume transports, the correlation between the two configurations was high (0.99 for the total temperature transport) and the offset was small (0.05 PW for the total). Thus, we are confident that this approach provides a good compensation for the reduced mooring coverage and that undersampling due to three rather than four moorings is not a problem in combining and averaging the results from the various moored arrays.

The model results were used to calculate heat transports over the same area as the moorings and in a similar fashion. Again, the direct method was used, although

no further interpolation of the model results from the model grid was done.

Before directly comparing model results to those from our moorings and from other investigators, we note that the values used for the specific heat capacity and density vary slightly. We have used a product of 4.09773×10^6 J K^{-1} m^{-3} for the $C_p\rho$ product; the CME model results are based on a value of 4.186×10^6, Hall and Bryden (1982) use a value of 4.093×10^6, and M90 use a value of 4.1×10^6.

3. Results

a. Temperature transport variability

Observed and modeled temperature transport time series are shown in Figs. 4a (transport above and below 800 m) and 4b (baroclinic and barotropic transports). Time series statistics are presented in Table 1. Uncertainties in the mean temperature transport values are computed assuming an integral timescale of 60 days, based on the autocorrelation functions of the time series. The standard deviation is divided by the square root of the number of degrees of freedom in the time series, based on the above timescale, to obtain the standard error.

Before discussing the temperature transport variability, it is useful to consider the corresponding variations in volume transport through the moored section (Fig. 5). To first order, variations in temperature transport over the whole or part of the water column are governed by volume transport variations and, therefore, as noted previously, they have limited meaning for a section with nonzero volume transport. The conventional breakdown into barotropic and baroclinic heat transport components is intrinsically more useful, as this results in one component (the baroclinic) that is independent of volume transport and determined only by the vertical shear of the flow and a second (the barotropic) that contains the vertically integrated transport variation and requires a complete mass closure for interpretation.

The total volume transport through the moored section shows a large range of variability, from approximately 60 Sv northward to 80 Sv southward. Transport in the upper 800 m is predominantly northward, although reversals are frequently observed that can result in southward upper layer transports of up to about 20 Sv. Below 800 m the transport is generally southward with only occasional reversals, which have been shown by Lee et al. (1990) and LJZF to correspond to periods when the DWBC meanders offshore and an anticyclonic eddy develops near the western boundary that causes deep northward flow shoreward of the DWBC. The transport variations above and below 800 m show similar timescales, and exhibit a high degree of correlation, indicating that much of the transport variability is barotropic. Transport variations in the lower layer (below 800 m) dominate the total transport and are typically 2–4 times larger than the upper layer transport variations.

Conversely, temperature transport variability (Fig. 4a) is primarily concentrated in the upper layer, due to the warmer temperatures associated with the upper flow. As with volume transport, variability can be seen on several different timescales; the largest events appear to occur on roughly a 70 to 100 day scale. Changes can often be rapid, taking place over a few days to a week. Mean temperature transports above and below 800 m are 0.37 and -0.39 PW, respectively, relative to 0°C, with ranges from -1.69 to 2.96 PW above 800 m, and -0.94 to 0.54 PW below. The mean value of the total temperature transport, considering all three deployments, is fairly small at -0.02 PW, with a year-to-year variability of about 0.2 PW (Table 1).

Separating the temperature transport into baroclinic and barotropic components shows that the several month timescale variations contain about equal parts of baroclinic and barotropic heat transport within the coherent section. The barotropic heat transport is primarily negative, with a range of -2.02 to 2.31 PW and a mean of -0.56 ± 0.14 PW, dominated by mean southward flow in the DWBC. An important finding is that while the overall baroclinic heat flux for the entire transatlantic section is southward (M90 give a value of -0.160 PW), we observe a strong northward mean baroclinic heat transport of 0.54 ± 0.07 PW in the Abaco section, with a range of -0.53 to 1.92 PW. As previously noted, this value is independent of volume transport or temperature reference, and its large positive value is due to the strong shear between the northward flowing Antilles Current and the southward flowing DWBC that are contained within our moored arrays in the mean.

As a check on the moored estimates, temperatures and geostrophic velocities calculated from CTD profiles taken along the Abaco transect were used to compute the baroclinic heat transports. Except for occasions when the transports were changing rapidly, baroclinic heat transports derived from moored and CTD sections were in very good agreement (Fig. 4b).

Inspection of the time series (Figs. 4 and 5) reveals similar scales of variability in the model and the moored estimates. The model temperature transport is overall more northward than the observed temperature transport due to the weaker thermohaline circulation and stronger wind-driven circulation off Abaco in the model. The observed volume transport over the coherent section is -22.2 Sv, with 5.2 Sv above 800 m and -27.4 Sv below, while the model volume transport is -5.7 Sv, with 12.0 above 800 m and -17.6 Sv below.

Variance conserving spectra computed from these time series are shown in Figs. 6a–e. They bear a very strong resemblance to the volume transport spectra shown in LJZF, with the most prominent peak around 70–140 days and a secondary peak around 20–30 days. Much of this energy is concentrated in the upper layer above 800 m. The ''100-day'' peak is best defined in

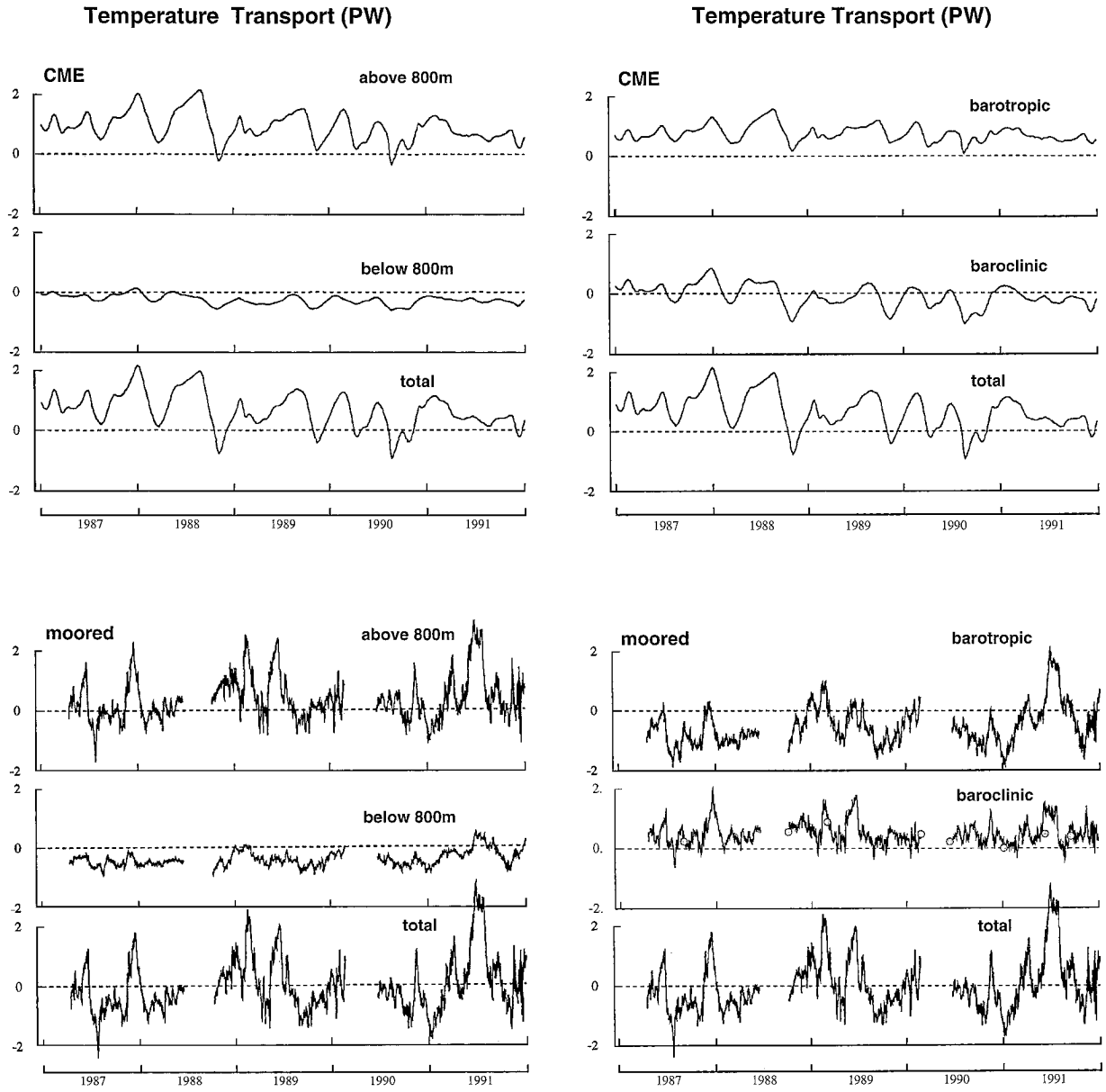

FIG. 4. (a) Time series of temperature transport (PW) over the coherent section. Upper panel is model results; lower is moored results (top: above 800 m; middle: below 800 m; bottom: total temperature transport). (b) Same as in Fig. 4a but for barotropic (top), baroclinic (middle), and total (bottom). Additional points on middle panel are from CTD sections.

the baroclinic spectrum (Fig. 6d) and the upper 800 m (Fig. 6b), and is only observed below 800 m during STACS-8. LJZF found that the 100-day variability in the upper 800 m was dominated by wavelike baroclinic eddies propagating westward into the Bahamas boundary from the interior.

b. Model derived temperature transport variability versus section width

The concentration of temperature transport variability in western boundary currents was investigated by integrating the temperature transport over progressively longer sections from the model data, starting at the Bahamas and extending eastward. The objective was to determine the section length necessary to reduce the variability to nominal levels. Standard errors are computed in the same way as for the observed data; that is, the standard error of the temperature transport over a given part of the section is calculated as the standard deviation of the respective model time series divided by the square root of the degrees of freedom.

The standard error of temperature transport for the model analog to the coherent array section (85 km),

TABLE 1. Abaco heat transport time series statistics (PW) over the coherent array for all mooring deployments and for the CME model. The total number of points and the range of values are also shown.

Deployment	Mean	Timespan: Std err	Timespan: Min	Timespan: Max	Number of points: Range
STACS-8	17 Apr 1987–19 Jun 1988				859
Total	−0.325	0.253	−2.376	1.797	4.174
Above 800 m	0.141	0.222	−1.689	2.230	3.919
Below 800 m	−0.466	0.050	−0.940	−0.126	0.814
Baroclinic	0.483	0.128	−0.527	1.918	2.445
Barotropic	−0.808	0.155	−1.859	0.310	2.170
STACS-10	9 Oct 1988–23 Feb 1990				1006
Total	0.126	0.285	−1.421	2.538	3.959
Above 800 m	0.533	0.240	−0.825	2.508	3.333
Below 800 m	−0.407	0.077	−0.915	0.084	1.000
Baroclinic	0.616	0.133	−0.299	1.810	2.109
Barotropic	−0.489	0.206	−1.788	1.035	2.83
WATTS	24 Jun 1990–1 Jan 1992				1113
Total	0.077	0.342	−1.820	3.432	5.252
Above 800 m	0.401	0.263	−1.118	2.956	4.074
Below 800 m	−0.325	0.096	−0.872	0.541	1.414
Baroclinic	0.516	0.105	−0.364	1.483	1.848
Barotropic	−0.439	0.283	−2.015	2.308	4.323
All deployments	17 Apr 1987–1 Jan 1992				2978
Total	−0.022	0.180	−2.376	3.432	5.808
Above 800 m	0.371	0.146	−1.689	2.956	4.645
Below 800 m	−0.393	0.048	−0.940	0.541	1.482
Baroclinic	0.540	0.071	−0.527	1.918	2.445
Barotropic	−0.562	0.138	−2.015	2.308	4.323
CME model	4 Jan 1987–1 Jan 1992				600
Total	0.671	0.107	−0.919	2.151	3.070
Above 800 m	0.913	0.086	−0.329	2.156	2.485
Below 800 m	−0.242	0.028	−0.589	0.139	0.729
Baroclinic	0.751	0.049	0.093	1.570	1.477
Barotropic	−0.080	0.067	−1.012	0.851	1.863

using all five years of model data, is 0.107 PW, while that for the entire interior section from the Bahamas to Africa is 0.025 PW, about four times smaller. Lengthening the section to correspond to the entire WATTS section (out to 74°W—an additional 200 km) yields a standard error 0.073 while extending it a farther 300 km out to 71°W reduces the error to 0.052. Lengthening the section yet farther yields an uncertainty of 0.021 at 50.6°W. However, some care must be taken with this approach, as extending the section over the Mid-Atlantic Ridge causes the variability to rise again. It can clearly be seen that the major portion of the model variability occurs in the western boundary area. The fact that variability drops as the section length is increased implies that some compensation takes place in the interior for the large variability seen in the western boundary region.

c. *Spatial structure of eddy heat flux and temperature transport*

The eddy heat flux is here defined as

$$C_p\rho \int \int \langle \tilde{v}\tilde{\theta} \rangle \, dx \, dz, \tag{5}$$

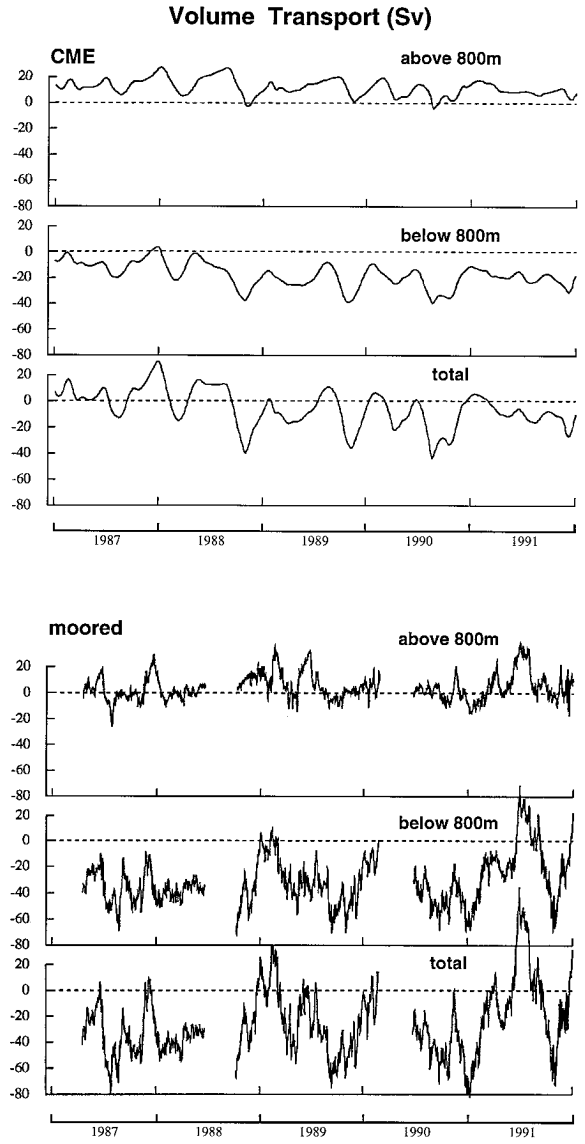

FIG. 5. Volume transport (Sv) for the Abaco section: Upper panel is model results, lower is moored results. (top: above 800 m, middle: below 800 m, bottom: total volume transport).

where the tildes represent deviations of the variables from their long-term means and the angle brackets denote a time average. This quantifies the meridional heat flux due to temporal correlation between the velocity and potential temperature fluctuations.

The spatial structure of the average eddy heat flux ($\langle \tilde{v}\tilde{\theta} \rangle$) and mean temperature transport $\langle v \rangle \langle \theta \rangle$ (over all three deployments) are shown in Figs. 7a and 7b, respectively. Northward temperature transport and northward eddy heat flux are concentrated against the Bahamas boundary in the upper 800 m, associated with the mean Antilles Current and its fluctuations, as well as warm anomalies that propagate into the Bahamas boundary from the interior. These features cause in-

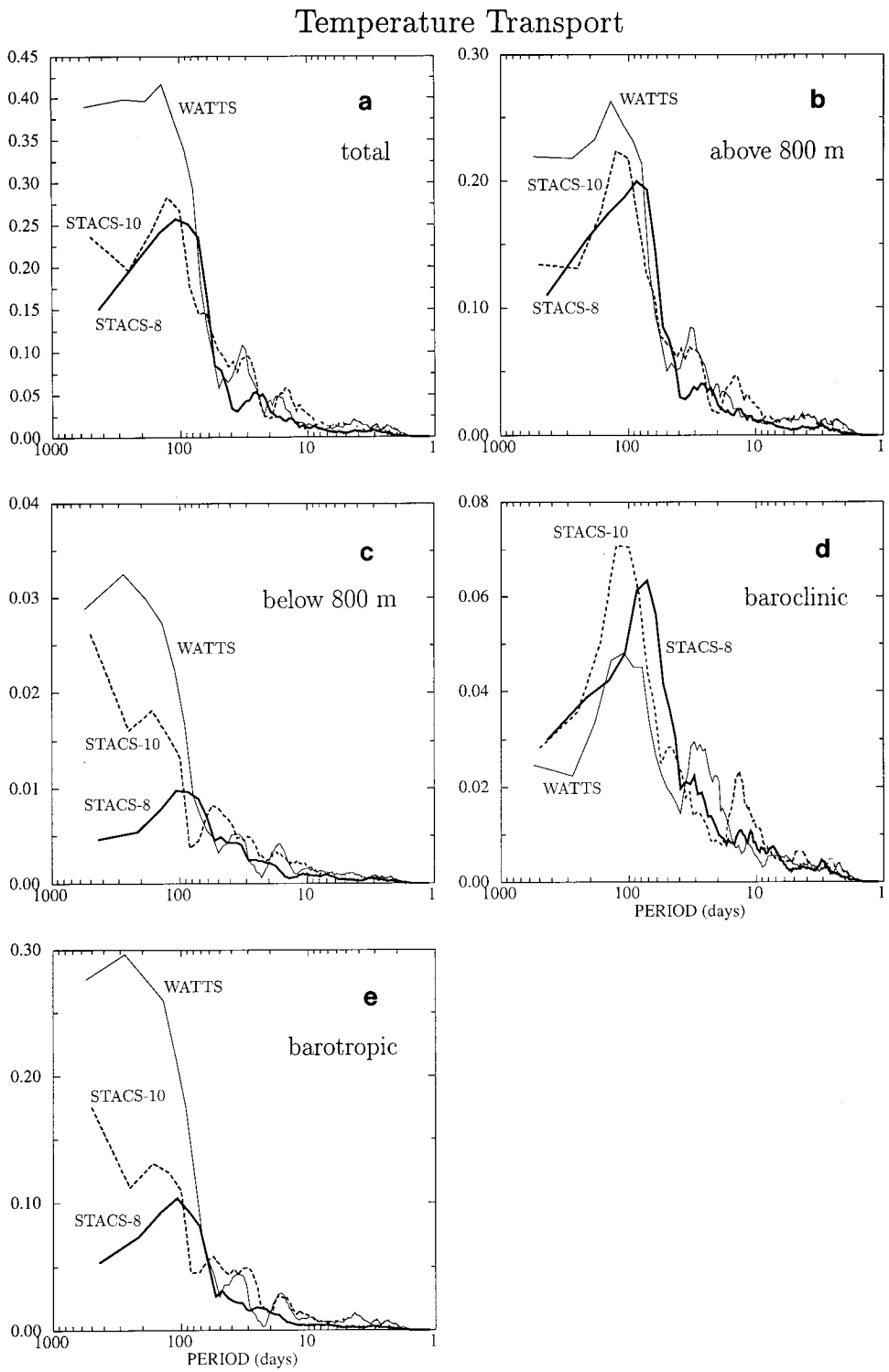

FIG. 6. Variance-conserving spectra of temperature transport time series: STACS-8 (bold), STACS-10 (dashed), and WATTS (solid). (a) Total transport; (b) above 800 m; (c) below 800 m; (d) baroclinic; (e) barotropic.

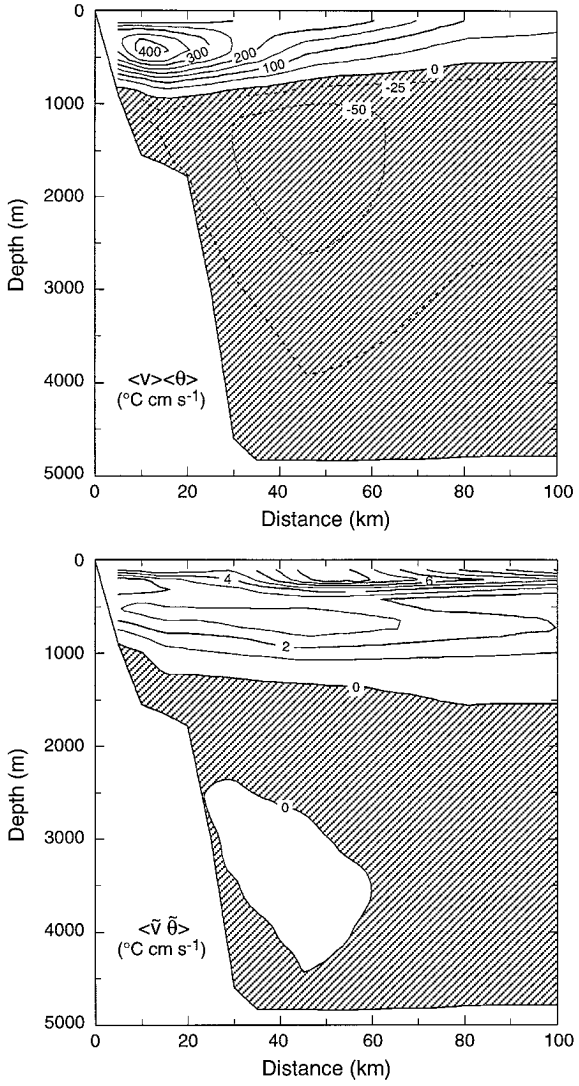

FIG. 7. Top: Temperature transport-average $\langle v\rangle\langle\theta\rangle$ cross section. Bottom: Eddy heat flux average $\langle\tilde{v}\tilde{\theta}\rangle$ cross section. Units are cm s^{-1} × °C. Averages are taken over all three deployments.

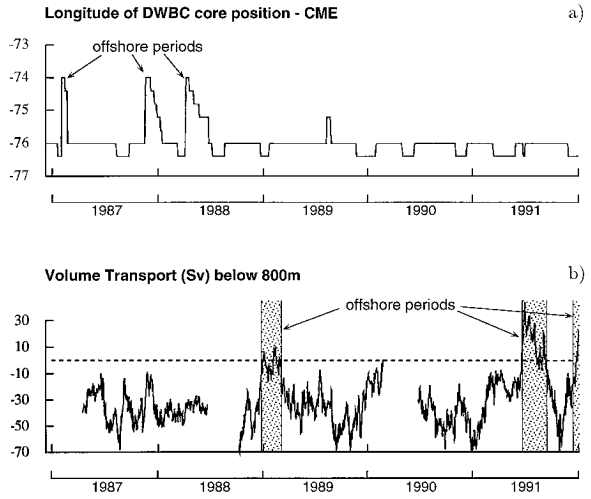

FIG. 8. Offshore meanders of DWBC. (a) Position of DWBC core in CME model; offshore events marked; (b) Moored estimate of volume transport below 800 m; offshore periods of the DWBC core are marked.

creased northward flow and warming, giving rise to the positive heat flux. Below 800 m the temperature transport is negative due to the southward flow of the DWBC and much weaker than in the thermocline because of the lower temperatures. The eddy heat transport is also much weaker below the thermocline (95% of the average eddy heat transport is above 800 m). As the mean eddy heat flux is only 0.012 PW, even in this energetic area, it appears negligible elsewhere in the transatlantic section.

d. Onshore/offshore positions of DWBC

LJZF found that periods of weak southward or even northward deep transport occur when the core of the DWBC meanders offshore of the coherent array. An attempt was made to determine the offshore meander times so they could be excluded from averaging periods. This should provide a more representative estimate of the actual mean temperature transport and its baroclinic/barotropic components occurring over the full width of the fluctuating western boundary layer. Offshore meandering was investigated in the CME model by tracking the position of the volume transport maximum below 800 m (assumed to be the DWBC core) (Fig. 8a). Brief offshore excursions occurred to a longitude of about 74°W, or approximately the eastern edge of our coherent array. However, the core normally remained within the array. From the moored observations, offshore meander periods were identified by LJZF and excluded from the transport time series averaging (Fig. 8b). These offshore meander periods appeared reasonably similar between the model and moored data, in terms of frequency of occurrence (three events over five years in both cases), duration (one to three months), and distance of meander (offshore to about 74°W).

Temperature transport statistics were recomputed after removal of the offshore meander periods (Table 2). The STACS-8 statistics are unchanged, as there was no adjustment during this time. Removing the offshore meander periods caused a decrease in northward temperature transport in the upper 800 m and an increase in southward temperature transport below 800 m. The net effect on the 4.8-yr average total temperature transport is a change from −0.02 to −0.21 PW, primarily due to an increase in southward barotropic transport. The baroclinic heat transport is quite robust and remains essentially unchanged by the meander removal (from 0.54 to 0.53 PW). A similar correction to the temperature transports derived from the CME model produced a much smaller change in the mean values because of the weaker DWBC in the model, and because the tendency

TABLE 2. Heat transport statistics (PW) over the coherent array with the effect of offshore meanders of the DWBC removed.

Deployment	Mean	Std err	Min	Max	Number of points Range
STACS-8					859
Total	−0.325	0.253	−2.376	1.797	4.174
Above 800 m	0.141	0.222	−1.689	2.230	3.919
Below 800 m	−0.466	0.050	−0.940	−0.126	0.814
Baroclinic	0.483	0.128	−0.527	1.918	2.445
Barotropic	−0.808	0.155	−1.859	0.310	2.170
STACS-10					857
Total	−0.039	0.270	−1.421	2.014	3.435
Above 800 m	0.429	0.240	−0.825	2.420	3.246
Below 800 m	−0.468	0.067	−0.915	0.009	0.925
Baroclinic	0.599	0.143	−0.299	1.810	2.109
Barotropic	−0.638	0.186	−1.788	0.450	2.238
WATTS					881
Total	−0.264	0.251	−1.820	1.896	3.716
Above 800 m	0.175	0.202	−1.033	2.114	3.147
Below 800 m	−0.439	0.070	−0.872	−0.071	0.801
Baroclinic	0.500	0.098	−0.282	1.483	1.765
Barotropic	−0.764	0.193	−2.015	0.574	2.589
All deployments					2597
Total	−0.210	0.151	−2.376	2.014	4.390
Above 800 m	0.248	0.131	−1.689	2.420	4.109
Below 800 m	−0.458	0.037	−0.940	0.009	0.950
Baroclinic	0.527	0.080	−0.527	1.918	2.445
Barotropic	−0.737	0.104	−2.015	0.574	2.589
CME model					565
Total	0.635	0.109	−0.919	2.151	3.070
Above 800 m	0.893	0.089	−0.329	2.156	2.485
Below 800 m	−0.259	0.027	−0.589	0.136	0.725
Baroclinic	0.746	0.051	0.093	1.570	1.477
Barotropic	−0.111	0.066	−1.012	0.851	1.863

for northward eddy flow to occur near the western boundary during observed offshore meanders was less pronounced in the model. This removal of the major offshore meander periods largely eliminates undersampling of the DWBC from the mean values and gives a better picture of long-term transports in the western boundary region.

e. Barotropic correction to transatlantic heat flux

In previous works (Hall and Bryden 1982), heat flux calculations were performed assuming that barotropic flows in the interior occur at a uniform temperature equal to the basin-averaged mean temperature $\langle\bar{\theta}\rangle$, assumed constant across the basin (approximately 5.5°C for the Atlantic at 26.5°N). However, in shallow regions with strong currents such as the area off the Bahamas, this assumption will cause an error in the heat flux estimate, as the strong local currents amplify the effect of the local vertically averaged temperature that tends to be warmer than the transect mean. The barotropic correction term (BT_{cor}) is defined here as the difference between the barotropic temperature transport and the value that would be obtained for the barotropic transport if the constant temperature $\langle\bar{\theta}\rangle$ is used instead of the actual instantaneous local vertical mean temperature. That is,

$$BT_{cor} = C_p\rho\left\{\int H\bar{v}\bar{\theta}\,dx - \langle\bar{\theta}\rangle\int H\bar{v}\,dx\right\}, \qquad (6)$$

where the overbars indicate vertical averages.

The average $v\theta$ distribution for each array deployment shows that the maximum northward temperature transport is located over a small shelf that breaks the steep Bahamas Escarpment at depths of about 900 to 1500 m (Fig. 7), which can give rise to significant barotropic correction to the total heat transport.

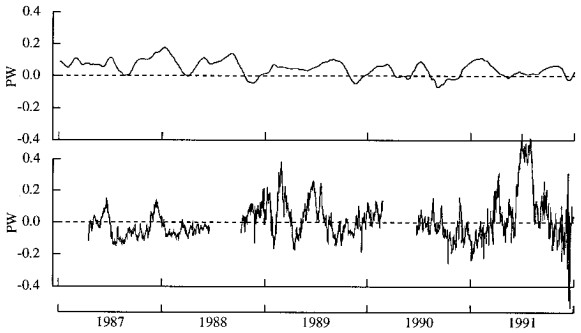

FIG. 9. Time series of the barotropic correction term to heat transport (PW) over the Abaco array; model results above, mooring results below.

Time series of this barotropic correction term were made from the moored data and the model (Fig. 9). These time series show that the barotropic correction term is indeed important in the shallow boundary currents off the Bahamas and can be a sizeable fraction of the entire transatlantic heat flux (up to nearly 30% of the total). Comparison with volume transport time series (Fig. 5) indicates that the variability of the barotropic correction term is controlled by volume transport changes in the upper 800 m. The barotropic correction term is large at times of maximum northward volume transport, which occurs when warm anomalies reach the Bahamas boundary and the DWBC shifts offshore. Model time series of the barotropic correction term off Abaco have about half the observed amplitude but share similar timescales. Similar calculations done using CME model data over the Mid-Atlantic Ridge and off the coast of Africa show that the barotropic correction term is much smaller there (especially over the Mid-Atlantic Ridge) and probably negligible (see Table 3).

The important point here is that, while the long-term average of the barotropic correction term is small [we estimate a value of 0.01 PW; Hall and Bryden (1982) estimate a value of 0.04 PW, while M90 reported a value of 0.03 PW], the instantaneous value can be quite large and has large variability, which means that the heat flux values made instantaneously (rather than as mean values) must include this contribution to the total heat flux.

TABLE 3. Barotropic correction term from moored arrays (PW) near Abaco compared to total barotropic heat transport and total heat transport in shallow regions of the Mid-Atlantic Ridge (MAR) and African coast from the CME model.

	Mean	Error	Min	Max	Range
			Moored array		
STACS-8 correction	−0.036	0.022	−0.147	0.154	0.301
STACS-10 correction	0.041	0.034	−0.185	0.385	0.570
WATTS correction	0.028	0.054	−0.534	0.563	1.097
			CME model		
Abaco correction	0.049	0.009	−0.071	0.176	0.247
Barotropic total	−0.080	0.067	−1.012	0.851	1.863
Total heat transport	0.671	0.107	−0.919	2.151	3.070
West MAR correction	−0.009	0.002	−0.040	0.024	0.064
Barotropic total	−0.116	0.014	−0.256	0.102	0.358
Total heat transport	−0.204	0.017	−0.455	0.094	0.549
East MAR correction	0.001	0.004	−0.034	0.066	0.100
Barotropic total	0.010	0.019	−0.180	0.322	0.501
Total heat transport	−0.081	0.031	−0.396	0.499	0.895
African coast correction	−0.025	0.002	−0.054	−0.003	0.051
Barotropic total	−0.100	0.011	−0.237	0.019	0.256
Total heat transport	−0.220	0.017	−0.422	−0.013	0.409

f. Annual cycle

The annual cycles of temperature and volume transport through the Abaco array area were calculated, using all available mooring data (STACS-8, STACS-10, and WATTS) and all five years of model data. Monthly averages were computed for the total water column, above and below 800 m, and for the baroclinic and barotropic components. As for the record means, these monthly means were corrected for offshore meander periods by excluding those periods from the monthly averaging.

The resulting annual cycles of the total temperature transport, its barotropic and baroclinic components, and total volume transport are shown in Figs. 10a–d, after smoothing with a 3-month running filter. Envelopes on the curves show the ± 1 standard error bars. (Note that all annual cycles shown here and subsequently in section 4, including relevant results from M90, are computed by smoothing the original monthly mean values with a running 3-month filter to reduce month-to-month variability and emphasize the seasonal variation.) The model and mooring cycles generally have a similar pattern, although there appears to be a phase shift of approximately 2 months, such that the moored cycles lead those of the model. The model cycles are also shifted toward stronger northward transports as a result of the model's weaker thermohaline circulation and tend to have a smaller annual range (e.g., approximately 0.5 PW for the total temperature transport, as compared to 0.7 PW from the moorings). The shift between the CME annual cycle and that derived from the moorings averages 0.6 PW for the total temperature transport. Most of the difference (0.5 PW) is accounted for in the transport above 800 m; in both the CME model and the moored data the annual cycle in temperature transport is dominated by the contribution above 800 m (not shown). While the standard errors associated with the monthly means indicate that significant interannual variability is present, the existence of an annual cycle is still readily apparent.

For the volume and total temperature transport (Figs. 10a and 10b), the model shows a winter maximum and a fall minimum, reminiscent of the annual transport cycle predicted by Anderson and Corry (1985) in their wind-forced basin model. The model also shows a secondary maximum in the summer and a secondary minimum in the spring. The observed annual cycle of temperature transport is qualitatively similar to that predicted by the CME model, with a late spring–early summer maximum of 0.2 PW and fall minimum of -0.5 PW. However, the winter maximum is somewhat less in the moored measurement as compared to the model prediction and, as noted before, leads in phase by about 2 months.

For both the model and moored data the baroclinic and barotropic components of the temperature transport have similar annual cycles, and both contribute roughly equally to the annual cycle of the total temperature transport (Figs. 10c and 10d). However, the semiannual variation in the observed temperture transport is contained almost entirely in the baroclinic component, whereas in the model it occurs with nearly equal amplitude in both components. We note that the temperature transport cycle is similar to the volume transport cycle in both the model and moored data, indicating that the annual changes in temperature transport are primary due to seasonal changes in the strength of the boundary currents. LJZF conclude that forcing for the annual cycle is caused mainly by changes in interior wind stress over the basin, producing a predominantly barotropic response in the western boundary region similar to that predicted by Sverdrup theory, with a lesser role played by local forcing.

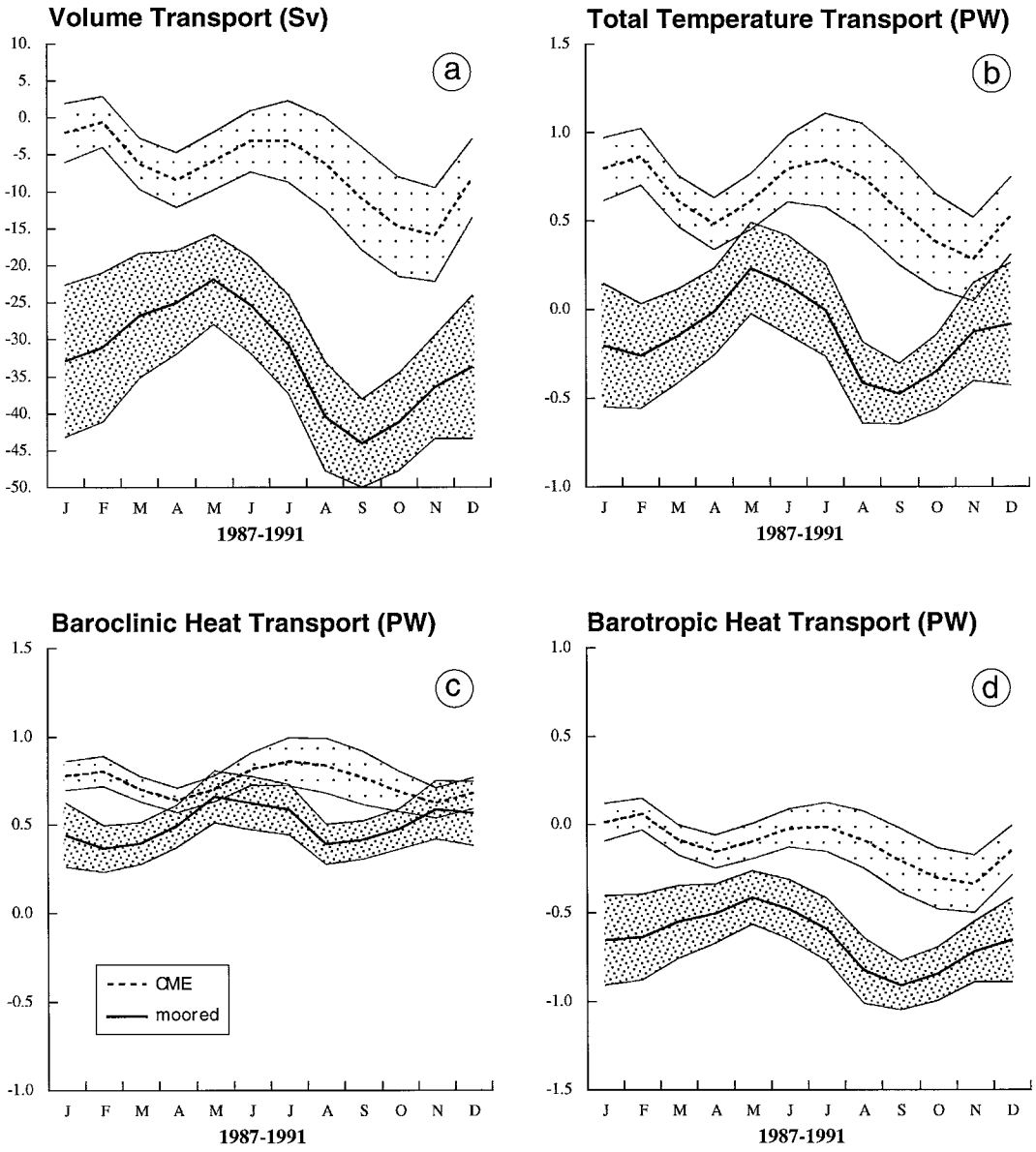

FIG. 10. Annual transport cycles (offshore DWBC meanders have been removed from averaging) for Abaco data (solid) and CME model (dashed), smoothed over 3 months. The envelope given shows the standard error. (a) Volume transport (Sv); (b) total temperature transport (PW); (c) baroclinic heat transport (PW); (d) barotropic heat transport (PW).

The annual cycle of volume transport shown here was computed from the 4.8-yr period from 1987 to 1992, whereas the volume transport annual cycle shown by LJZF (their Fig. 16) was computed from a 5.8-yr time series from 1986 to 1992. The first year of data (1986–87) is excluded here because it consisted of only one complete mooring and was not suitable for heat transport calculations. The two realizations of the annual cycle are qualitatively similar, although the longer time period (5.8 yr) annual cycle more closely follows the phasing of the model annual cycle. This indicates that interannual variability can be significant and points to the need for long time series to adequately resolve the climatological annual cycle in such energetic regions.

4. Discussion

a. Transatlantic heat flux

A new estimate of net transatlantic heat flux and its seasonal variability is made here by combining monthly averaged heat transports from our moored time series (using all three deployments and excluding offshore DWBC meander periods) with the Levitus climatology data used by M90.

Differences in the present study compared to that of M90 are as follows: First, we combine the annual cycles of barotropic temperature transport and volume transport observed from our Abaco moored data with the corresponding annual cycles of the Florida Current from M90 and then balance the smaller mass residual with the interior flux. M90's treatment of the Abaco region consisted of applying a mean barotropic correction for the area based on a limited number of sections with no annual variation. Second, we use the baroclinic heat transports calculated from the Abaco array to improve the estimate in the western boundary layer, which is not well resolved by Levitus, while M90 uses only the Levitus climatology.

Following the breakdown used by M90, the total barotropic heat transport is given by

$$Q_{\mathrm{bt}} = Q_{\mathrm{btFS}} + Q_{\mathrm{btA}} - C_p\rho(V_{\mathrm{FS}} + V_{\mathrm{A}})\theta_I, \qquad (7)$$

where Q_{btFS} and Q_{btA} are the Florida Straits and Abaco barotropic heat transports, V_{FS} and V_{A} are the corresponding Florida Straits and Abaco volume transports, θ_I is the mean interior temperature, and all values except those for Abaco are taken from M90. M90 estimated the seasonal cycle of the barotropic heat transport for the Florida Current by combining section data across the Straits of Florida near 26°N (Niiler and Richardson 1973; Brooks 1979) and near 27°N (Leaman et al. 1987), obtaining annual mean values of 30.6 ± 2.8 Sv for the volume transport and 2.04 ± 0.19 for the associated barotropic heat transport (from M90's Table 5). Use of the Leaman et al. (1987) data alone at 27°N leads to slightly larger mean values of 31.7 ± 3.0 Sv and 2.18 ± 0.24 PW. This difference probably reflects the additional transport joining the Florida Current between 26° and 27°N through the Northwest Providence Channel [estimated at 1.2 Sv by Leaman et al. (1995)], which should properly be accounted for in the 26.5°N heat flux estimate. However, the above estimates are not significantly different within the error bars, and no seasonal cycle is available for the Leaman et al. (1987) data. We therefore retain M90's seasonal estimates for the Florida Current, while noting that the use of Leaman et al.'s mean values, after accounting for the additional 1.1 Sv returning at the interior mean temperature, would increase our final estimate of the annual-mean transatlantic heat flux by approximately 0.1 PW.

Our annual cycle and total barotropic heat flux using the Abaco data (Fig. 11b) are very similar to the M90 barotropic heat flux (an annual average of 1.35 PW versus M90's 1.37 PW). The close agreement in mean value

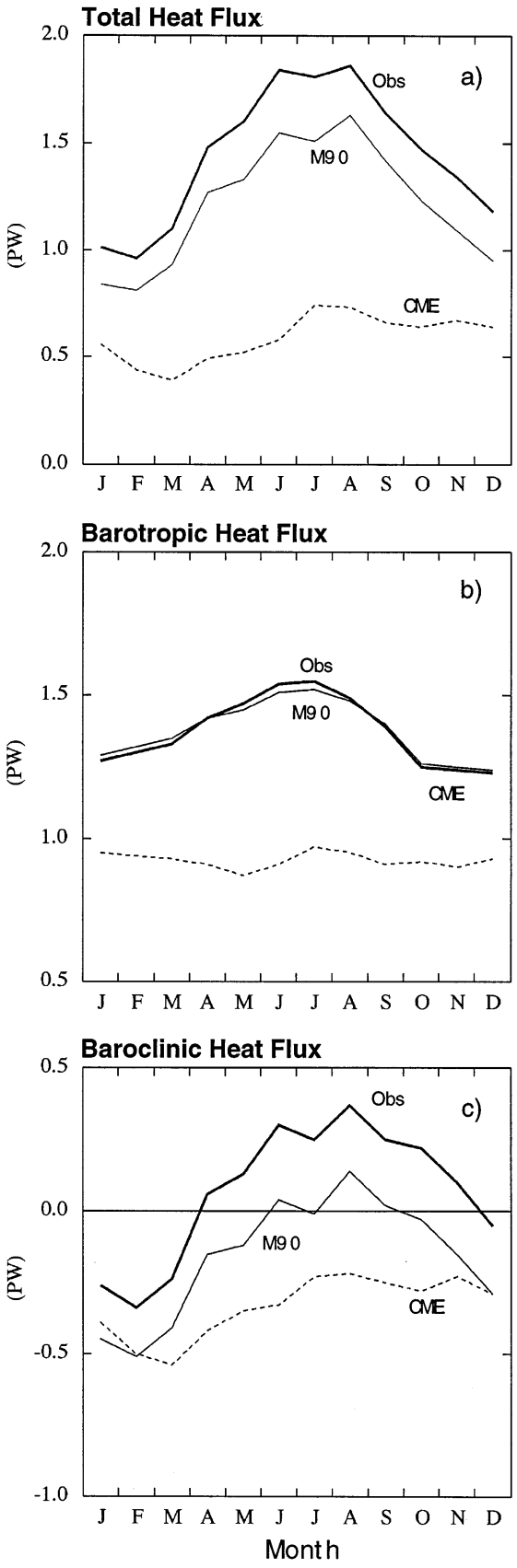

→

FIG. 11. Monthly averages (smoothed over 3 months) of the total transatlantic heat flux (PW) from Levitus climatology (M90), climatology plus Abaco moored observations (Obs), and from the CME model for (a) total heat flux, (b) barotropic heat flux, and (c) baroclinic heat flux.

is not unexpected, as any differences are mainly due to the barotropic correction term off Abaco, which has a small overall average value of 0.01 PW (M90 used 0.03 PW). The only difference in the annual cycle is a slight increase in the summer maximum (approximately 0.1 PW greater than the M90 result) and a corresponding decrease in the winter (Fig. 11b). This difference is due to a seasonal increase in the northward transport over the Bahamian slope in summer, as noted by LJZF, at relatively warm temperatures.

The total meridional baroclinic heat flux Q_{bc} across 26.5°N was computed by combining the Florida Straits baroclinic heat transport Q_{bcFS}, the interior baroclinic heat transport Q_{bcI}, and the Abaco mooring section baroclinic transport Q_{bcA}. The Ekman transport Q_{Ek} as given by M90 is also included here.

Thus, the baroclinic heat flux is given by

$$Q_{bc} = Q_{bcFS} + Q_{bcA} + Q_{bcI} + Q_{Ek}, \quad (8)$$

where Q_{bcI} is the interior baroclinic heat transport calculated from Levitus excluding that portion in the western boundary region off Abaco, represented by Q_{bcA}.

The Levitus climatology is on a one-degree grid; monthly values are available to 1000 m, and annual averages below. Merging of our moored baroclinic heat transport estimates with the Levitus climatology is not a straightforward procedure, due to sampling differences between the two datasets. In particular, we find a substantial difference in the baroclinic heat transport estimate off Abaco from these data sources. While M90 found an annual mean contribution to the interior baroclinic heat flux of only 0.11 PW in the westernmost 1° bin of the interior from Levitus, the moored estimates of baroclinic flux in this area (see Table 2) from STACS-8, STACS-10, and WATTS are 0.48 ± 0.13, 0.60 ± 0.14, and 0.50 ± 0.10 PW, respectively. The overall average is 0.54 ± 0.07 PW, or nearly five times the value from the Levitus climatology. Extending the integrated area of the Levitus hydrographic data out to 3° from the western boundary increases this value to 0.2 PW, which is still less than half the moored estimate. This suggests that the smoothing employed in the Levitus climatology underestimates the northward heat transport in the Antilles Current region close to the Bahamas. A comparison of the seasonal cycles from Levitus (for the first degree and first three degrees of the interior) and from the moorings (not shown) shows that this offset occurs throughout the year rather than being concentrated in any particular season.

Hydrographic sections made at 24.5°N (Fig. 12) also show a larger northward baroclinic heat transport in the west than the Levitus climatology would indicate (larger than 0.5 PW within 2° of the western boundary), again suggesting that the use of the Levitus climatology produces a total baroclinic heat flux that is too strong in a southward sense. The transatlantic baroclinic heat flux from the IGY section (Oct 1957) is −0.877 PW, while the October baroclinic heat flux from Levitus climatology at 24.5°N is −1.084 PW, a difference of 0.21 PW. Similarly, the June/July 1981 *Atlantis II* section baroclinic heat flux is −0.781 PW, while the average of the June and July results from the climatology is −0.893 PW, a difference of 0.11 PW. The annual average climatological result at this latitude is −0.985 PW. While not conclusive, this does imply that the Levitus climatology tends to overestimate the interior southward baroclinic heat flux.

We believe the main reason for this is a lack of resolution in the western boundary region due to smoothing and averaging of the hydrographic data into 1° squares. At 26.5°N, the westernmost Levitus data bin is centered at 76.5°W, half a degree from the western boundary. Thus, averaging of hydrographic data over 1° squares, even without the further smoothing employed by Levitus, potentially results in the transport through the half-degree nearest shore being unresolved, where the Antilles Current and much of the DWBC are confined (LJZF and Fig. 7). Accordingly, the baroclinic heat transport in this region due to the shear between these strong opposing flows could be significantly underestimated. To account for this sampling deficiency near the western boundary, two approaches were used in attempting to combine the Abaco and Levitus data. The first consists of simply substituting the moored array estimates for the westernmost 1° bin of the interior from Levitus, which, for reasons to be discussed shortly, probably leads to an overestimate of the transatlantic heat flux. The second attempts to include only that portion of the western boundary baroclinic heat transport unaccounted for by Levitus, while retaining the full interior contribution calculated from the Levitus data.

Substituting in the Abaco baroclinic heat transports for the western one-degree bin of Levitus data results in an increase of about 0.4 PW for the annually averaged interior baroclinic heat flux at 26.5°N, from −0.84 PW to −0.41 PW. Monthly values increase by 0.2 to 0.6 PW, with the largest increase during the summer maximum and the smallest during the winter minimum (not shown). That the overall interior baroclinic heat flux is really 0.4 PW larger seems doubtful, since this is more than twice the difference between the seasonal Levitus values and those calculated from individual sections just a few degrees farther south (Hall and Bryden 1982; Roemmich and Wunsch 1985). One potential problem with this approach is that it attempts to patch a well-resolved result in the western boundary layer into a highly smoothed climatology. Assuming that the main effect of smoothing in the Levitus climatology is to spread the influence of the boundary currents toward the interior, this could lead to a portion of the boundary currents being counted twice. As shown in M90 (see also Fig. 12), the region of northward baroclinic heat transport in the Levitus data associated with the boundary current system off Abaco extends about 4° offshore, before reversing to southward heat transport in the interior. Most of the northward heat transport (95%) is

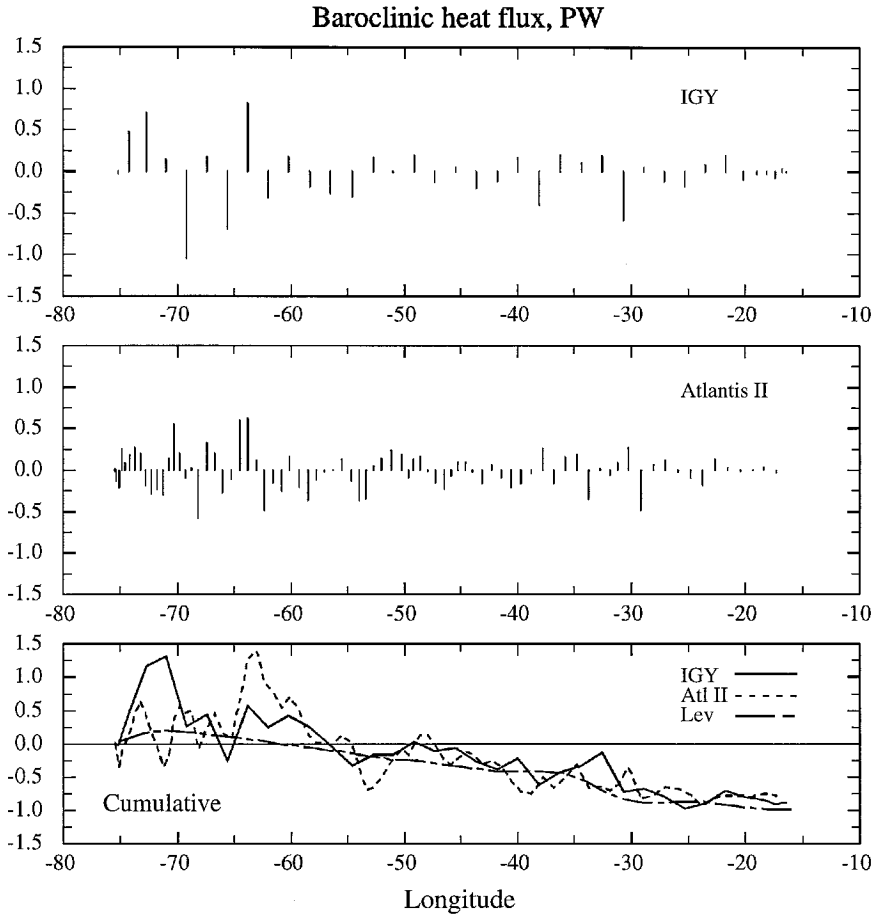

FIG. 12. Transatlantic section (at 24.5°N) baroclinic heat flux (PW) from the IGY (1957) and *Atlantis II* (1981) transects. Baroclinic heat flux from Levitus climatology at this latitude is also shown.

contained in the first 3° from the western boundary. Replacing this portion of the Levitus data with the moored results leads to a smaller increase in the total interior baroclinic heat flux of 0.32 PW. While probably more reasonable, this approach could still lead to an overestimate of the total interior baroclinic heat transport if the southward baroclinic heat transport offshore of the western boundary layer due to gyre return flow is significantly reduced by being smoothed with the signature of the western boundary current. This is of particular concern for the Abaco region because the mean flow offshore of the Antilles Current and DWBC is characterized by relatively strong southward flow in the upper ocean associated with Gulf Stream recirculation, and underlying northward deep flow related to DWBC recirculation (Lee et al. 1990; LJZF). The southward baroclinic heat transport in this area and the opposing northward heat transport in the western boundary layer would thus be mutually weakened by the Levitus averaging process and neither would be adequately resolved. It is therefore difficult to determine at what location, if any, it is appropriate to patch the Abaco results into the Levitus interior data.

As an alternate approach, we utilize the full Levitus interior baroclinic heat transport as Q_{bcI} in (8) and assume that the main quantitative effect of the Levitus averaging is to exclude the contribution occurring in the half-degree nearest shore, between Abaco and 76.5°W. Therefore, estimates from the western portion of the array, out to 76.5°W, are used as Q_{bcA} in (8) rather than those from the full width of the coherent array. This increases the monthly values of the total interior baroclinic heat transport by 0.2 to 0.3 PW over that derived from Levitus, and the annual average by 0.23 PW to −0.61 PW. This approach is used in the final calculations on total transatlantic heat flux reported here.

The annual cycle of the total transatlantic baroclinic heat flux, after combination with the remaining terms in (8) from M90, is shown in Fig. 11c and Table 5. The total annually averaged baroclinic heat flux across 26.5°N is 0.07 PW, with maximum baroclinic heat flux in summer and minimum in fall and winter.

TABLE 4. Monthly average of transatlantic barotropic heat flux (PW) using western half of Abaco moored estimates with offshore meanders removed together with M90 estimates. All monthly values are smoothed with a 3-month running filter. See text for definition of terms.

Month	Q_{btFS}	F_{FS} (Sv)	Q_{btA}	V_A (Sv)	θ_I (°C)	Q_{bt} M90	Q_{bt}
Jan	1.91	28.67	−0.21	−9.45	5.50	1.29	1.27
Feb	1.95	29.13	−0.19	−8.90	5.49	1.32	1.30
Mar	2.02	30.73	−0.18	−8.39	5.49	1.35	1.33
Apr	2.13	32.47	−0.14	−7.10	5.50	1.42	1.42
May	2.17	33.03	−0.08	−5.49	5.51	1.45	1.47
Jun	2.24	33.33	−0.06	−5.48	5.52	1.51	1.54
Jul	2.25	33.43	−0.11	−7.45	5.54	1.52	1.55
Aug	2.19	32.37	−0.22	−11.16	5.54	1.48	1.49
Sep	2.06	30.03	−0.26	−12.25	5.54	1.40	1.39
Oct	1.86	27.63	−0.24	−11.39	5.53	1.26	1.25
Nov	1.85	27.67	−0.20	−9.83	5.53	1.25	1.24
Dec	1.85	28.10	−0.19	−9.26	5.52	1.24	1.23
Annual	2.04	30.55	−8.84	−0.17	5.52	1.37	1.37

A consistent treatment of the barotropic heat flux, in which Q_{btA} and V_A in (7) are calculated over only the western part of the Abaco array, and the residual mass transport ($V_{FC} + V_A$) is again balanced with interior transport, leads to negligible changes in the barotropic heat flux results. The annual average value is 1.37 PW (identical to M90's result) versus our 1.35 PW using the full Abaco array. (Table 4 presents the monthly mean values, smoothed over three months; the Q_{btFS} values listed there include the −0.11 PW barotropic correction term for the Florida Current given by M90.)

The annual cycle of the total meridional heat flux across 26.5°N is estimated from the sum of the baroclinic and barotropic components (Fig. 11a and Table 5). The total heat flux is maximum in the summer and minimum in the winter and fall. The range of the annual cycle is 0.82 PW for the M90 data and 0.90 PW when the Abaco moored data are included, an increase of approximately 0.1 PW. The sum total annual heat flux including Abaco data is then 1.44 PW, compared to the M90 value of 1.21 PW.

Uncertainty in our new estimate of transatlantic heat flux comes from uncertainties in both the Abaco moored estimate and the M90 result. For the Abaco array, the 0.18 PW standard error (over all deployments) is assumed to be the dominant uncertainty; errors in the measured temperatures and velocities and in the methodology used should be insignificant (on the order of 0.05 PW or less) compared to the uncertainty from time variability. M90 estimated that the uncertainties in each heat transport component are 0.12 PW for the barotropic heat transport, 0.16 PW for the interior baroclinic heat transport, 0.06 PW for the Florida Straits baroclinic heat transport, and 0.10 PW for the Ekman transport. Additionally, they include 0.24 PW uncertainty from the eddy heat flux. Based on our observation of a small (negligible) contribution to the eddy heat flux in the western boundary layer, we assign a maximum value of 0.1 PW to this uncertainty. We also include a 0.1 PW error to account for uncertainties in the merger of our Abaco data with the interior Levitus data to estimate the total interior baroclinic heat transport. Combining all these (by the standard propagation of uncertainties method that involves taking the square root of the sum of squares of errors) gives a total uncertainty of ±0.33 PW for the 1.44 PW average.

While it might seem tempting to perform a similar calculation using a hydrographic section instead of a

TABLE 5. Monthly averages of transatlantic baroclinic heat flux (PW) using western half of Abaco moored estimates with offshore meanders removed in addition to interior values from M90. All monthly values, including those taken from M90, are smoothed with a 3-month running filter. The total heat flux is also shown here.

Month	Q_{bcFS}	Q_{bcI}	Q_{bcA}	Q_{Ek}	Q_{bc}	Q_{bc} M90	Q_t M90	Q_T
Jan	0.32	−1.03	0.19	0.26	−0.26	−0.45	0.84	1.01
Feb	0.29	−0.99	0.17	0.19	−0.34	−0.51	0.81	0.96
Mar	0.30	−0.93	0.18	0.22	−0.24	−0.41	0.93	1.10
Apr	0.34	−0.77	0.21	0.29	0.06	−0.15	1.27	1.48
May	0.36	−0.83	0.25	0.34	0.13	−0.12	1.33	1.60
Jun	0.38	−0.72	0.26	0.38	0.30	0.04	1.55	1.84
Jul	0.38	−0.80	0.26	0.41	0.25	−0.01	1.51	1.81
Aug	0.39	−0.70	0.23	0.45	0.37	0.14	1.63	1.86
Sep	0.36	−0.78	0.23	0.44	0.25	0.02	1.42	1.64
Oct	0.30	−0.77	0.25	0.44	0.22	−0.03	1.23	1.47
Nov	0.30	−0.86	0.25	0.41	0.10	−0.15	1.09	1.34
Dec	0.30	−0.93	0.23	0.35	−0.05	−0.29	0.95	1.18
Annual	0.33	−0.84	0.23	0.35	0.07	−0.16	1.21	1.44

climatological section and inserting the mooring results at the western end, this method is not practical. First, the nearest presently available transatlantic sections (the 1957 IGY section and the 1981 *Atlantis II* section) are at 24.5°N, 2° south of the Abaco mooring site, where the topography is quite different. The Antilles Current extends significantly farther east at 24.5°N, and the DWBC is also farther east, as can be seen from hydrographic sections previously shown.

Even if a transatlantic section at 26.5°N existed, clipping out its westernmost stations and substituting mooring data would be a dubious proposition at best, for it would be difficult to match the eddies. Note how different the baroclinic heat flux in the westernmost regions of the IGY and *Atlantis II* sections (Fig. 12) are, even though the total section baroclinic heat flux agrees within 0.1 PW for the two sections (baroclinic heat flux is −0.78 PW for the IGY section and −0.88 PW for the *Atlantis II* section), while the baroclinic heat flux in the westernmost segment of the section from 75.5° to 72.75°W is 1.17 PW for IGY and 0.46 PW for *Atlantis II*.

The issue of just how to best construct a transoceanic heat flux estimate from partial section direct observations and climatologies is still a matter that requires further study. The construction of climatologies with considerably less smoothing in the western boundary region than that employed by Levitus is recommended in future studies to help avoid the matching problems we have encountered.

b. Modeled and observed heat transports

The annual cycle of transatlantic heat flux calculated directly from the CME model is also shown in Fig. 11, along with its breakdown into barotropic and baroclinic components. It can be seen in Fig. 11a that in addition to having a too weak annual mean heat flux, the model has a much weaker annual cycle than indicated by observations. The reasons for the lower mean value are known (Bryan and Holland 1989) and can be attributed primarily to an inadequacy in the ''sponge layer'' boundary conditions that drive the large-scale overturning cell in the model. However, it is not obvious why the annual cycle in the model should be so small compared to observations, which in a sense might be considered an even more fundamental disagreement. To clarify the reasons for these differences, it is instructive to break down the model heat transport into component terms using the same methodology that is applied to observations.

The annual mean heat flux in the model is just 0.59 PW at this latitude, somewhat less than half of the observed value. As discussed by Bryan et al. (1995) the meridional overturning cell in the model is 7–10 Sv too weak in midlatitudes, which largely accounts for this difference. As shown in Figs. 11b and 11c, the shortfall in the total heat flux in the model is divided roughly equally between the barotropic (0.45 PW) and baroclinic (0.40 PW) heat flux components, yielding a total difference of 0.85 PW. This result may seem odd, since one normally associates an overturning cell entirely with the baroclinic circulation (Böning and Herrmann 1994). The partitioning has to do with the somewhat nonphysical definitions of these quantities used in the observation-based approach. The dominant contribution to the barotropic heat flux in (7) is

$$Q_{\rm bt} = C_p \rho V_{\rm FS} (\theta_{\rm FS} - \theta_I), \tag{9}$$

where $V_{\rm FS}$ is the volume transport of the Florida Current, and $\theta_{\rm FS}$ and θ_I are the mean temperatures of the Florida Current and the interior, respectively (Fig. 13a). A signature of the weaker thermohaline cell in the model is that the mean Florida Current transport is only 22.8 Sv, or approximately 8 Sv smaller than observed (M90; Leaman et al. 1987). This leads to a reduction in $Q_{\rm bt}$ of 0.25 PW, for the model mean temperatures $\theta_{\rm FS} = 14.7$°C and $\theta_I = 5.6$°C. The remainder of the difference between the modeled and observed $Q_{\rm bt}$ is due to the fact that the mean Florida Current temperature in the model is about 2°C cooler than observed (M90 find $\theta_{\rm FS} = 17$°C), which leads to a further $Q_{\rm bt}$ deficit of 0.2 PW in the model. (The interior mean temperature in the model of 5.6°C is very close to the 5.5°C value M90 calculated from the Levitus climatology.) The remaining heat transport difference is contained in the baroclinic component, which is smaller (larger southward) in the model due to an increase in the basin-averaged southward vertical shear across the interior. This follows from the weaker DWBC in the model, which, when coupled with the upper ocean southward gyre flow, leads to a stronger overall southward shear. The baroclinic heat flux associated with northward vertical shear in the Florida Current is similar in both model and observations, with the CME actually having a slightly larger value (0.4 PW versus 0.33 PW).

Now consider the annual cycles. The observed barotropic, baroclinic, and total heat flux have similar annual cycles with a maximum in summer and a minimum in fall or winter (Fig. 11a). The CME shows a weak annual cycle for the baroclinic heat flux that is roughly in phase with observations but almost no variation in the barotropic heat flux. The reason for the weak annual cycle in barotropic heat flux in the model is illustrated in Fig. 13a. Variations in the barotropic heat flux are related primarily to changes in the volume transport and mean temperature of the Florida Current, following (9). The observed cycle (Fig. 11a) is primarily driven by the annual cycle in Florida Current volume transport, which varies over a range of 6 Sv (Fig. 13a). By comparison, the CME annual Florida Current transport cycle is much weaker, about one-third the observed amplitude, and with somewhat different phase. Both cycles have a fall minimum, but the summer maximum in the observed transport is only weakly evident in the model. Furthermore, the annual cycle of the mean Florida Cur-

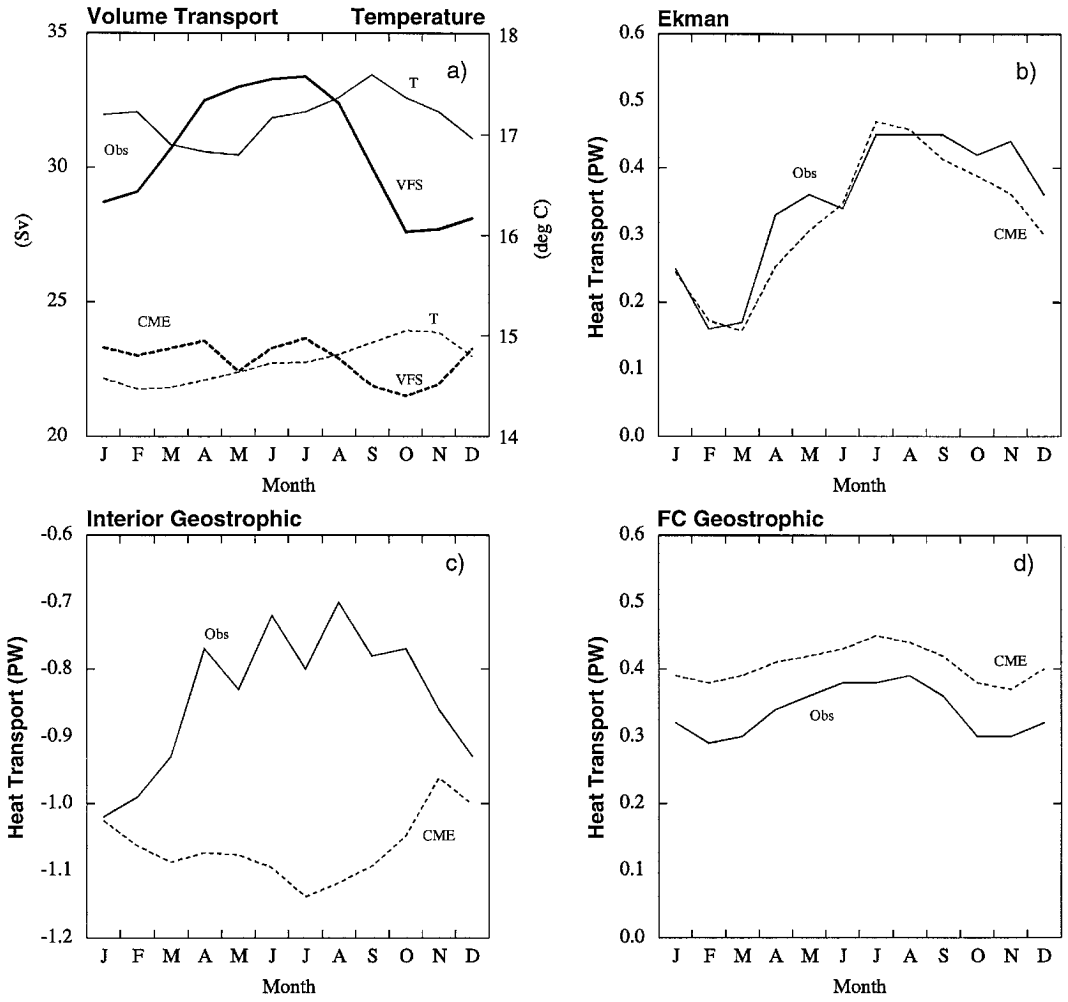

FIG. 13. Individual terms in transatlantic heat flux calculation, from observations and the CME model. (a) Florida Straits monthly average volume transports (V_{FS}) and potential temperatures (T); (b) Ekman heat transport; (c) interior baroclinic heat transport due to geostrophic flow; and (d) Florida Straits baroclinic heat transport (in PW); observations are solid lines, model is dashed.

rent temperature in the model is nearly out of phase with the transport, such that the effect of the fall transport minimum is largely suppressed by the fall maximum in temperature. A similar cycle is seen in the observed temperature, but it has a much smaller net effect due to the dominance of the volume transport cycle.

Annual cycles of the various components of the baroclinic heat flux (Q_{Ek}, Q_{bcI}, and Q_{bcFS}) are shown in Figs. 13b–d. The annual cycles of the Ekman and Florida Current contributions are very similar between the observations and model. (It is not possible to precisely calculate the Ekman contribution in models or data due to uncertainty in the depth of the Ekman layer and hence in the bulk temperature associated with that flow. Here we have simply calculated it from the model as the residual of the directly calculated interior baroclinic heat flux and the geostrophic contribution.) The major discrepancy between the model and observations is in the contribution due to interior geostrophic flow, where their annual cycles are essentially out of phase. The model annual cycle has a weak (southward) minimum in summer, whereas the observed annual cycle, calculated from Levitus climatology, has a broad maximum in summer with nearly three times the amplitude (annual range of approximately 0.3 PW). Böning and Herrmann (1994) found the CME annual heat flux cycle at subtropical latitudes to be almost completely due to the Ekman contribution. This result is consistent, as they point out, with theoretical and modeling studies indicating that there is little baroclinic adjustment of the gyre circulation on the annual timescale due to the very slow propagation of baroclinic Rossby waves at midlatitudes. In view of this, the relatively large amplitude of the observed baroclinic heat flux cycle is puzzling. The sense of the variation is such that there is larger southward baroclinic shear in the interior during winter, which suggests an intensification of the southward upper ocean gyre flow during winter, when the wind stress

curl and resulting southward Sverdrup transport are at their maxima. This relationship suggests a baroclinic response to Sverdrup forcing, which is at odds with the model results. It is not immediately clear that the CME model is necessarily incorrect; indeed, it is possible that due to irregular sampling and eddy contamination, the Levitus annual climatology may not be representative of the true interior annual cycle. In either case, a fundamental disagreement between model and observational data seems to exist on the amplitude of annual variation in the interior baroclinic heat flux, which needs to be reconciled by further study.

The overall result of the nearly in-phase Ekman, Florida Current, and interior contributions in the observations is a relatively large annual range of 0.7 PW in the total baroclinic heat flux. Conversely, the interior geostrophic contribution in the model tends to oppose the Ekman contribution, leading to a much smaller annual range of 0.3 PW.

In summary, we conclude that the weakness of the annual cycle of meridional heat flux in the CME relative to observations is primarily due to 1) the weak annual cycle of the Florida Current, and 2) the lack of a substantial geostrophic heat flux variation in the interior.

5. Conclusions

The results from a long-term current meter array have been used to investigate heat transport off the Bahamas at 26.5°N and their impact on transatlantic heat flux. This location is important for accurate measurement of the meridional heat transport, because it lies within both the latitude band of maximum heat flux and the high-energy western boundary current region.

Time series of local temperature transport off Abaco are highly variable and are dominated by volume transport variations. The variability occurs on timescales ranging from weekly to interannual, including a prominent annual cycle. Heat transport is locally strong both northward (primarily in the upper layer above 800 m, due to the Antilles Current and baroclinic events) and southward (especially below 800 m, where the velocity and temperature structure is more barotropic, caused mainly by the DWBC).

Volume and temperature transport fluctuations are concentrated on roughly a 100-day timescale, and smaller amplitude variations are observed on monthly timescales. The large 70 to 100-day events masked the annual cycle in earlier observations taken over one to three year periods; however, it is now possible to resolve an annual cycle from our 4.8 years of data. This annual cycle, with a summer maximum and fall minimum, is in good qualitative agreement with that predicted by the CME model. While the model's volume and heat transports are, in general, weaker than those observed, the model amplitudes and timescales of variability are quite similar to the observed.

Monthly averages of Abaco moored heat transports were used in combination with Levitus climatology in the interior and Florida Current and Ekman transports as given by Molinari et al. (1990) to estimate seasonal and annual cycles of transatlantic heat flux. Barotropic, baroclinic, and total heat flux had similar annual cycles with a summer maximum and a fall and winter minimum.

The baroclinic heat transports computed with the addition of the moored estimates were about 0.2 PW larger than those computed from Levitus climatology; this result caused a similar increase in the total transatlantic heat flux ranging from a maximum of 1.9 PW in August to a minimum of 1.0 PW in February. The annual mean heat flux was 1.44 PW (0.23 PW larger than the M90 estimate) when including the moored estimates. The 0.23 PW increase in net heat flux appears to be associated with the large northward heat transport of the Antilles Current, which is confined close to the Bahamas boundary as a narrow shallow jet and not properly accounted for in the climatological dataset.

Comparisons of the transatlantic heat flux calculated from observations and from the CME model show that, for the barotropic component, the CME's weaker overall heat flux and weaker annual cycle are related to its cooler and weaker Florida Current. Differences in the baroclinic component are primarily reflected in the interior geostrophic portion of the heat flux, which shows a larger annual cycle in the Levitus data than in the model.

Moored current meter observations continue off Abaco, designated as the WOCE ACM-1 transport monitoring site. The most recent recovery and redeployment occurred in October 1995; thus, there are now more than nine years of nearly continuous data available from the area. Study of long-term variability and trends in the regional transports will continue.

Acknowledgments. CME data were kindly provided by Frank Bryan at NCAR; time on the NCAR Cray was contributed through NCAR Project 35191048. We thank John Festa for monthly baroclinic heat transports calculated from Levitus climatology for the ocean interior and for results from the IGY and *Atlantis II* sections as used in M90. Doug Luther provided helpful comments on the manuscript and brought to our attention the differences between the M90 and Leaman et al. (1987) estimates of Florida Current heat transport. Funding for this research was provided by NOAA/AOML under Cooperative Agreement NA85-WC-H-06314 with the Cooperative Institute of Marine and Atmospheric Studies (associated with University of Miami/RSMAS), National Science Foundation Grant OCE 8911859, NOAA Atlantic Climate Change Program Grant NA37RJ0200, and partial support as a component of the U.S. contribution to the international WOCE.

REFERENCES

Akima, H., 1970: A new method of interpolation and smooth curve fitting based on local procedures. *J. Assoc. Comput. Mach.,* **17,** 589–602.

Anderson, D. L., and R. A. Corry, 1985: Seasonal transport variations in the Florida Straits: A model study. *J. Phys. Oceanogr.,* **15,** 773–786.

Böning, C.W., and P. Herrmann, 1994: On the annual cycle of poleward heat transport in the ocean: Results from high resolution modeling of the North and Equatorial Atlantic. *J. Phys. Oceanogr.,* **24,** 91–107.

——, R. Doscher, and R. Budich, 1991a: Seasonal transport variation in the western subtropical North Atlantic: Experiments with an eddy-resolving model. *J. Phys. Oceanogr.,* **21,** 1271–1289.

——, ——, and H. Isemer, 1991b: Monthly mean wind stress and Sverdrup transport in the North Atlantic: A comparison of the Hellerma–-Rosenstein and Isemer–Haas climatologies. *J. Phys. Oceanogr.,* **21,** 221–235.

——, W. Holland, F. Bryan, G. Danabasoglu, and J. McWilliams, 1994: An overlooked problem in model simulations of the thermohaline circulation and heat transport in the Atlantic Ocean. *J. Climate,* **8,** 515–523.

Brooks, I. H., 1979: Fluctuations in the transport of the Florida Current at periods between tidal and two weeks. *J. Phys. Oceanogr.,* **9,** 1048–1053.

Bryan, F., 1986: High-latitude, salinity effects and interhemispheric thermohaline circulations. *Nature,* **323,** 301–304.

——, and W. Holland, 1989: A high resolution simulation of the wind and thermohaline-driven circulation in the North Atlantic Ocean. *Parametrization of Small-Scale Processes, Proc. Aha Huliko'a Hawaiian Winter Workshop.* P. Müller and D. Anderson, Eds., University of Hawaii at Manoa, 99–115.

——, C. W. Böning, and W. Holland, 1995: On the midlatitude circulation in a high-resolution model of the North Atlantic. *J. Phys. Oceanogr.,* **25,** 289–305.

Bryan, K., 1962: Measurements of meridional heat transport by ocean currents. *J. Geophys. Res.,* **67,** 3403–3414.

——, 1969: A numerical method for the study of the circulation of the world ocean. *J. Comput. Phys.,* **4,** 347–376.

Bryden, H. L., and M. M. Hall, 1980: Heat transport by currents across 25°N latitude in the Atlantic Ocean. *Science,* **207,** 884–886.

——, D. H. Roemmich, and J. A. Church, 1991: Ocean heat transport across 24°N in the Pacific. *Deep-Sea Res.,* **38,** 297–324; Suppl., 39–53.

Cox, M. D., 1985: An eddy-resolving numerical model of the ventilated thermocline. *J. Phys. Oceanogr.,* **15,** 1312–1324.

Hall, M. M., and H. L. Bryden, 1982: Direct estimate and mechanism of ocean heat transport. *Deep-Sea Res.,* **29**(3A), 339–359.

Han, Y.-J., 1984: A numerical world ocean general circulation model. Part II: A baroclinic experiment. *Dyn. Atmos. Oceans,* **8,** 141–172.

Hellerman, S., and M. Rosenstein, 1983: Normal monthly wind stress over the world ocean with error estimates. *J. Phys. Oceanogr.,* **13,** 1093–1104.

Leaman, K. D., and J. E. Harris, 1990: On the average absolute transport of the deep western boundary currents east of Abaco Island, the Bahamas. *J. Phys. Oceanogr.,* **20,** 467–475.

——, R. L. Molinari, and P. S. Vertes, 1987: Structure and variability of the Florida Current at 27°N: April 1982–July 1984. *J. Phys. Oceanogr.,* **17,** 565–583.

——, P. S. Vertes, L. P. Atkinson, T. N. Lee, P. Hamilton, and E. Waddell, 1995: Transport, potential vorticity, and current/temperature structure across Northwest Providence and Santaren Channels and the Florida Current off Cay Sal Bank. *J. Geophys. Res.,* **100,** 8561–8570.

Lee, T. N., W. Johns, F. Schott, and R. Zantopp, 1990: Western boundary current structure and variability east of Abaco, Bahamas at 26.5°N. *J. Phys. Oceanogr.,* **20,** 446–466.

——, ——, R. Zantopp, and E. Fillenbaum, 1996: Moored observations of western boundary current variability and thermohaline circulation at 26.5°N in the subtropical North Atlantic. *J. Phys. Oceanogr.,* **26,** 962–983.

Levitus, S., 1982: *Climatological Atlas of the World Ocean.* NOAA Prof. Paper 13, U.S. Govt. Printing Office, 173 pp.

Manabe, S., and R. J. Stouffer, 1988: Two stable equilibria of a coupled ocean–atmosphere model. *J. Climate,* **1,** 841–866.

Molinari, R. L., E. Johns, and J. F. Festa, 1990: The annual cycle of meridional heat flux in the Atlantic Ocean at 26.5°N. *J. Phys. Oceanogr.,* **20,** 476–482.

Niiler, P. P., and W. S. Richardson, 1973: Seasonal variability of the Florida Current. *J. Mar. Res.,* **31,** 144–167.

Roemmich, D., and C. Wunsch, 1985: Two transatlantic sections: Meridional circulation and heat flux in the subtropical North Atlantic Ocean. *Deep-Sea Res.,* **32,** 619–664.

Schmitz, W. J., J. D. Thompson, and J. R. Luyten, 1992: The Sverdrup circulation for the Atlantic along 24°N. *J. Geophys. Res.,* **97,** 7251–7256.

Vonder Haar, T. H., and A. H. Oort, 1973: New estimate of annual poleward energy transport by northern hemisphere oceans. *J. Phys. Oceanogr.,* **3,** 169–172.